AD-A040 640 CALIFORNIA UNIV LIVERMORE LAWRENCE LIVERMORE LAB F/G 17/9
THE DERIVATION OF SIMPLE POLES IN A TRANSFER FUNCTION FROM REAL--ETC(U)
JAN 77 E K MILLER, J N BRITTINGHAM W-7405-ENG-48
UNCLASSIFIED UCRL-52211-PT-3 NL

| OF |
ADA
040640

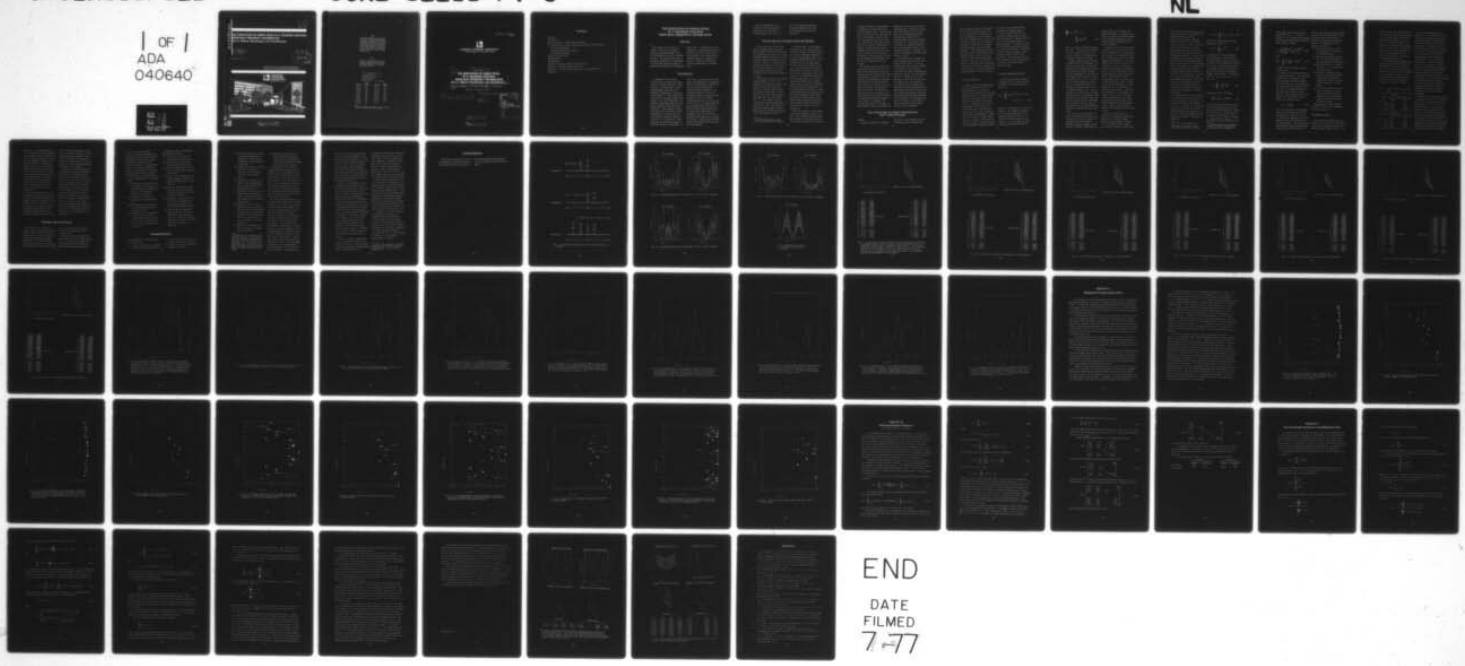

END

DATE
FILMED
7-77

B. S.

UCRL-52211

THE DERIVATION OF SIMPLE POLES IN A TRANSFER FUNCTION FROM REAL FREQUENCY INFORMATION

Part 3: Object Classification and Identification

E. K. Miller
J. N. Brittingham
E. L. Willows

January 10, 1977

Prepared for U.S. Energy Research & Development Administration under contract No. W-7405-Eng-48

LAWRENCE LIVERMORE LABORATORY
University of California/Livermore

Printed in the United States of America
Available from
National Technical Information Service
U.S. Department of Commerce
5285 Port Royal Road
Springfield, VA 22161
Price: Printed Copy $; Microfiche $3.00

Page Range	Domestic Price	Page Range	Domestic Price
001–025	$ 3.50	326–350	10.00
026–050	4.00	351–375	10.50
051–075	4.50	376–400	10.75
076–100	5.00	401–425	11.00
101–125	5.50	426–450	11.75
126–150	6.00	451–475	12.00
151–175	6.75	476–500	12.50
176–200	7.50	501–525	12.75
201–225	7.75	526–550	13.00
226–250	8.00	551–575	13.50
251–275	9.00	576–600	13.75
276–300	9.25	601–up	*
301–325	9.75		

*Add $2.50 for each additional 100 page increment from 601 to 1,000 pages; add $4.50 for each additional 100 page increment over 1,000 pages.

Distribution Category
UC-38

LAWRENCE LIVERMORE LABORATORY
University of California Livermore, California 94550

UCRL-52211 - Pt. 3

THE DERIVATION OF SIMPLE POLES IN A TRANSFER FUNCTION FROM REAL FREQUENCY INFORMATION. Part 3. Object Classification and Identification

E. K. Miller, J. N. Brittingham and J. L. Willows

MS date: January 10, 1977

10 Jan 77

W-7405-Eng-48

64 p.

Contents

THE DERIVATION OF SIMPLE POLES IN A TRANSFER FUNCTION FROM REAL FREQUENCY INFORMATION

Abstract

This report is the third in a series of three that evaluate a technique (frequency-domain Prony) for obtaining the poles of a transfer function. The main objective was to assess the feasibility of classifying or identifying ship-like targets by using pole sets derived from frequency-domain data. A predictor-correlator procedure for using spectral data and library pole sets for this purpose was developed. Also studied was an iterative method for reducing the effects of noise and a technique based upon magnitude-only spectral data.

Introduction

A technique for using real-frequency data to obtain the simple poles of a transfer function, and the results of its application to real electromagnetic (EM) data were described, respectively, in two previous reports.[1,2] The procedure was referred to as frequency-domain Prony because of its close similarity to a method of extracting poles from time-domain waveforms based upon Prony's technique.[3] First applied to specified pole sets to evaluate its characteristics[1] it was then used for real EM data to provide a more relevant test of its potential.[2] Some variations of the basic technique were also studied and described. In this work, our main objective was to assess the feasibility of classifying and/or identifying radar targets by use of pole data derived from frequency-domain information. We assumed the problem to be one of estimating whether an unknown object belongs to a class of concern (classification) and if so, which one of that class it is (identification). After obtaining some pole results derived from frequency-domain Prony for simple ship-like objects, we attempted to use such pole sets to establish which target from a library of pole sets is most like an unknown target whose scattered field spectrum has been obtained.

Results pertaining to 1) a "shifting" procedure applied to noisy data; 2) a vari-linear frequency-domain predictor; and 3) a pole extraction technique based upon magnitude-only data are discussed in the text and appendices.

Pole-set Results of Simple Ship-Like Models

In the first part of this study, before frequency-domain Prony had been developed, pole sets were derived from applying time-domain Prony to the computed transient waveform of several ship-like targets of increasing complexity.[4] Because of various uncertainties encountered in this effort,[4] it was deemed necessary to consider less-complex, targets while still retaining some features characteristic of ships.

Consequently, the series of simpler targets depicted in Fig. 1 were modeled in the frequency domain,* and their backscattered fields were obtained. Frequency spectra were calculated for two angles of incidence, 30° and 60°, with respect to the long axis of the wire models (Fig. 2). The straight wire was included for reference purposes at an angle of 60° only. The results of applying frequency-domain Prony to these spectra are summarized graphically and numerically in Fig. 3.

We observe that: 1) the greatest variations in pole values obtained for the two angles of incidence occur in their real (damping) components; 2) quite good agreement exists in the imaginary components of most of the two pole sets for the same target; 3) some poles do not appear in both sets, even though their invalidity is not indicated by either a small residue value or large negative real component; 4) the smooth pole trajectory of the straight wire is changed considerably by addition of the wires used in models 1-3; and 5) significant differences are also discernable in the backscatter-field spectra. These results demonstrate that the pole sets do contain potentially useful information for classifying and/or identifying radar targets but not without some uncertainty caused by possible discrepancies arising in the pole extraction.

The actual poles of a given object are uncertain primarily for two reasons. First, without knowing apriori what number of poles will contribute to the transfer function over a given

*Since frequency-domain Prony had been developed in the interim.

frequency interval, we over-estimate the number in the data when using frequency-domain Prony. This produces some curve-fitting poles which may not all be recognizable. Second, some pole locations may vary due to numerical inaccuracy as the problem parameters (e.g., angle of incidence) are changed, while others may totally disappear from the data because they are not excited for a given set of parameters. Noise, while not a factor in the computed data presented here, can also be responsible for such effects.

One approach to this problem that has worked especially well for noisy data in the time domain, should be equally useful for reducing the effects of parameter variations as well. By varying the parameters of the extraction process we can derive several sets of poles from the same data and then plot them on a single graph. When this is done, the valid poles are found to occur in clusters, and their positions can then be estimated by computing the mean coordinates of each cluster. In addition, the standard deviation of the points in each cluster can help to indicate the uncertainty in the location of that particular pole. Although not developed sufficiently for use in this study, some preliminary results of utilizing this technique with frequency-domain Prony are described in Appendix A. Our previous observation that the greatest variance in pole location usually occurs in the damping component is confirmed by the results of Appendix A and theoretical analysis as well.[5]

It is interesting to compare the lowest frequency poles for the four objects studied above. While the straight wire has a $j\omega$-axis component of 0.792 MHz, a lower value of 0.758 MHz occurs when an appendage is added near one end of the wire (ship-model 1). However, when the wire appendage is added at the center (as in ship-model 2), the resonance (0.788 MHz) is only slightly lower than the wire-only value because the appendage has little influence on the even current distribution characterizing the lowest-frequency resonance. For ship-model 3, the (average) resonance (0.751 MHz) is the lowest of the four because of the combined effects of both appendages.

Use of Pole Sets for Object Classification and/or Identification

GENERAL

A major motivation for studying the poles of radar targets is their potential use for classification

and/or identification (C/I) independent of aspect and polarization. As we have seen above, an appearance of aspect dependency can occur because some pole responses may not be excited at certain aspects and the computed locations of those that are excited may vary slightly with the problem parameters. This indicates an inherent uncertainty of indeterminant magnitude no matter how the poles or information derived from them might be used. Noise, of course, can be expected to increase this uncertainty. In any case, it would be expected that a common element of any pole-based C/I approach would be a pole-set library.

POLE-SET CORRELATION

Perhaps, the most straightforward way to use the pole sets in a C/I exercise would be to correlate directly the poles obtained from the scattered field of an unknown target with each of the pole sets in the library. This might be done optically, for example, by the use of transmission filters where the target-pole set is overlayed with each library set, and the relative correlation is established in proportion to the amount of light transmitted. A digital correlation technique could also be easily conceived, but this approach presupposes that a pole set will be derived from the spectrum of the unknown target.

Because we have found the pole extraction procedure may be numerically inconsistent, computation of the pole set from measured data is not always advisable. In addition, using the Prony technique requires substantial computing capability, and without access to a large computer, a near real-time target C/I may not be achievable. For these and other reasons, the direct use of the poles for C/I may not be the most useful approach to take.

A PREDICTOR-CORRELATOR APPROACH

An alternative has been tested in a transient format,[6] which involves the concept of a linear predictor of the form

$$f(t) = \sum_{n=1}^{N} a_{N,n}(-1)^{n+1} f(t - n \Delta t), \qquad t \geq N \Delta t, \tag{1a}$$

where N is the number of poles in the response. The predictor provides a way to obtain sampled values of a transient signal for all $t \geq T$ in terms of the given samples in the interval $t < T$, and a set of coefficients $a_{N,n}$ which are defined by

$$\prod_{\alpha=1}^{N} (s + e^{s_\alpha \Delta t}) = s^N + \sum_{\alpha=1}^{N} a_{N,\alpha} s^{N-\alpha}, \qquad (1b)$$

where s_α is the αth complex resonance (or pole). Note that for the predictor to be applied to a given f(t), the set of poles for the object that produced f(t) must be available.

Suppose, however, that the object is unknown and to be determined. If a library of pole sets is available, where one may correspond to the object from which f(t) has been obtained, then the coefficients of Eq. (1b) for each library pole set could be tried successively in Eq. (1a). In each case the known signal $f_k(t)$ would be used on the right hand side of the equation, which would lead to a set of computed signals $f_c(t)$. Upon comparison of $f_c(t)$ with $f_k(t)$ to establish the pole set that minimizes their difference, the reference target most like the unknown could be identified. This procedure would thus allow an identification to be made without the necessity of finding the poles from $f_k(t)$.[6]

The predictor just discussed is based on transient data while we are interesed in the use of spectral or frequency-domain information. Although a transient signal could be derived by Fourier transforming the spectral data, such an extra step seems unnecessary. It would be more direct to confine the process entirely to the frequency domain and find a frequency-domain equivalent of the linear predictor.

Although a direct frequency-domain analogue of Eq. (1) does not seem to exist, a procedure can be identified that operates in a strikingly similar way. To appreciate this, let us first examine the application of the time-domain linear predictor [Eq. (1)] in more detail. First, it requires a certain minimum amount of information before it can be implemented. For an N-pole system, the N-pole values are needed, which amounts to 2(N/2) = N-real numbers since the poles occur in complex conjugate pairs. Second, the N-resonance amplitudes, or their equivalent, are also required to specify the system fully. This introduces additional N-real numbers for a total of 2N. In Eq. (1), these resonance amplitudes are not explicitly involved but enter implicitly instead through the initial samples of f(t). Thus, from these 2N-real numbers we can obtain all other values of f(t).

Now let us consider what is required to develop an analogous procedure in the frequency-domain. Because the same amount of information is involved, 2N-real numbers will still be required. Again, this

might include the N-pole values, given by N-real numbers, while the other N numbers could come from the N-resonance amplitudes. Alternatively, as in Eq. (1), they could come from samples of $F(\omega)$. From this data, other $F(\omega)$ values could be derived for any ω value in the frequency range over which the 2N-real numbers were obtained. In this sense, a frequency-domain linear predictor differs from its time-domain counterpart, which applies for all subsequent time. Of course, if all system poles were available and used, then the frequency-domain version would also apply for all frequencies. Note also that successful application of the time-domain version does require that all poles contributing to f(t) be included in the linear predictor, so that use of the linear predictor for all time also requires all contributing poles.

A frequency-domain linear predictor could be written in the same way as Eq. (1); whereby, all $F(\omega)$ for $\omega > \omega_N$ are given in terms of $F(\omega)$ samples for $\omega < \omega_N$.* However, this is unnecessarily restrictive since we can generally predict and sample at relatively arbitrary frequencies over the spectrum of concern.† Therefore, we simply use

$$F(j\omega) = \sum_{\alpha=1}^{N} R_\alpha/(j\omega - s_\alpha). \quad (2a)$$

where the corresponding time-domain expression is given by

$$F(t) = \sum_{\alpha=1}^{N} R_\alpha e^{s_\alpha t}. \quad (2b)$$

Proceeding as for the time-domain linear predictor, assume that the N-complex-conjugate s_α are available. Then given N-real numbers from samples of $F(\omega)$, Eq. (2a) provides the basis for computing the as-yet unknown R_α. Suppose, for example, we are given measured real-frequency, complex samples** of $F(j\omega_k) = M_k$, $k = 1,\ldots,N$. Then from

$$M_k = \sum_{\alpha=1}^{N} X_{k_\alpha}^{(i)} R_\alpha^{(i)}, \quad (3a)$$

compute the vector $R^{(i)}$ where

$$X_{k\alpha}^{(i)} = \left(j\omega_k - s_\alpha^{(i)}\right)^{-1}, \quad (3b)$$

any N of the 2N-data points provided by the N-complex samples $M(j\omega_k)$ may be used, and the superscript i denotes the library pole set being employed. It should be noted that $R_\alpha = R^*_{\alpha+N/2}$, $s_\alpha = s^*_{\alpha+N/2}$ and $M_k = M^*_{k+N/2}$. If this process is performed for each of the

*This is shown in Appendix B.

†The actual ω used must satisfy the appropriate sampling criteria.

**Frequency-domain Prony currently requires both phase and amplitude data in general; see Appendix C.

M-pole sets in the library, then M vectors $R_\alpha^{(i)}$, i=1,..., M will be obtained. They by using the remaining N data points provided by the measured results $F(j\omega_k)$, compute

$$R_{xi} = \left(\frac{1}{N} \left| \sum_{k=1}^{N} \frac{M_k^{(i)} - M_k}{M_k} \right|^2 \right)^{1/2}, \quad (4a)$$

where

$$M_k^{(i)} = \sum_{\alpha=1}^{N} R_\alpha^{(i)} \Big/ \left(j\omega - s_\alpha^{(i)} \right), \quad (4b)$$

and $M_k^{(i)}$ and its complex conjugate are both used.

We refer to the overall process as a predictor-correlator. The subscript xi denotes R as a measure of similarity between the unknown target x and library entry i. The smaller R_{xi} is, the greater the similarity, and vice versa. A normalized version of R_{xi} that varies between 0 and 1, where the latter denotes perfect correlation, is perhaps more conventional, and we define it by

$$\hat{R}_{xi} \equiv \frac{1}{1 + R_{xi}} . \quad (4c)$$

Thus, by using part of the measured data to find a residue vector $R_\alpha^{(i)}$ corresponding to each pole set, we can predict the response at the other measured points and compare it with the actual values. The results giving best agreement with the measurements (smallest R_{xi}) establish that the pole set from which they were obtained is most like the unknown target, with statistical analysis necessary to establish confidence and probability bounds. The advantages of this approach are several:

- No pole sets need be derived from measured data obtained in an operational mode.
- The library pole sets required can be established under more favorable laboratory conditions.
- The excitation of all poles is unnecessary for the predictor-correlator to work.
- The entire operation is performed in the frequency domain, and generating time-domain information, either via transforms or directly, is unnecessary.
- It is well suited for analysis from an information-content viewpoint thus providing an opportunity for better understanding and more efficiently utilizing the data.

Some numerical results obtained from Eqs. (3) and (4) are summarized in the next section.

SOME NUMERICAL RESULTS

The procedure discussed above, as given by Eqs. (3) and (4), was applied to some of the ship-model data previously presented in Figs. 2 and 3. For

this test, the backscattered field of each ship-model was used successively as the unknown target return, while the library consisted of the pole sets of all three ship models. We used poles obtained for an incidence angle $\theta_I = 60,°$ while back scattered data for $\theta_I = 60°$ (case A) and 30° (case B) were employed for the predictor-correlator. The results are summarized in Table 1.

Some representative graphical data which depict the steps involved in implementing Eqs. (3) and (4) are shown in Fig. 4 for Case A. Plotted there is the total imput data spectrum for ship model 1, as well as those points used for the residue calculation [Eq. (3)] and the predictor-correlator [Eq. (4)]. Note that these two sets interleave in frequency, i.e., every other data point is used for the residue calculation, with the in-between points subsequently employed for the predictor-correlator. Following these plots are graphs that pertain to each pole set and show the predicted response and the difference in magnitude between the predicted and actual result, $|M_k^{(i)} - M_k|$. The latter, specifically, is useful in showing where, in the frequency spectrum covered, the differences between $M_k^{(i)}$ and M_k are largest, and thus where the discriminability between the various targets may be greatest. The possibility for establishing a measure of information content per-unit-frequency interval with respect to maximizing differences in target observables along these lines is interesting and deserves further examination.

Table 1. Target correlation matrices $\hat{R}_{xi}$.

Case A

	$\hat{R}_{xi}$	$\theta_{Poles} = 60°$;	$\theta_{RCS} = 60°$
x/i	1	2	3
1	1.000	0.329	0.637
2	0.316	1.000	0.701
3	0.523	0.536	1.000

Case B

		$\theta_{Poles} = 60°$;	$\theta_{RCS} = 30°$
x/i	1	2	3
1	0.760	0.330	0.389
2	0.235	0.561	0.340
3	0.461	0.531	0.736

Results for the correlation study are summarized in Table 1. We observe the $\hat{R}_{jj}$ has a value of unity for all three cases (i.e., j = 1, 2 or 3) in which the same θ_I is used for the pole and field calculation (Case A, Table 1). This shows that the predicted return matches that measured, when the pole set which corresponds to the target is used in Eq. (3). We expected this because the same target data was used to compute the respective pole sets and the correlation

number $\hat{R}_{jj}$. The corresponding $\hat{R}_{ij}$, $i \neq j$ values for this case, however, exhibit values that vary between ~0.3 and ~0.7, which establishes a measure of the dissimilarity between the three ship models. Note that the smallest $\hat{R}_{ij}$ values occur when the single-masted models are compared, which is a reasonable result when the geometrical differences between the three models are considered. Correlation of the two one-mast models with the two-mast model results in the larger $\hat{R}_{ij}$ values. Again, this agrees with what we might expect.

When the data used for the pole calculation are different from those to which the predictor-correlator is applied, then no $\hat{R}_{ij}$ values are unity (Case B, Table 1). Evidently, this is because of the slight variation in the poles which characterizes the different incidence angles, and occurs from current numerical limitations (as discussed earlier). However, we still find that $\hat{R}_{jj}$ for each target spectrum is largest. Presumably, by developing an internally consistent averaged pole set for each library entry, such angular-dependent variations could be reduced.

Although the technique presented above appears to have some potential for target C/I, considerably more effort would be necessary to make it practical. The effects of noisy data, aspect variations, accuracy of the library pole sets, etc., all need to be considered. In addition, other ways of computing R_{xi}, for example using the step-wise predictor described in Appendix B as an alternative to the approach described here, should be evaluated. More fundamentally, the information content of the available data should be explored as a means of establishing data requirements, error estimates, C/I confidence, etc.

Summary and Conclusions

This report is the third in a series of three which present results obtained from the initial phase of a program entitled "Radar Target Characterization via Complex Frequency Resonances." Our objective was to assess the feasibility of classifying or identifying (C/I) ship-like targets by use of radar returns relative to the complex resonances that characterize them.

Present test data do not confirm the feasibility but are highly encouraging. The basic tools required for this application, such as the pole-extraction (frequency-domain Prony)

technique, and the predictor-correlator, have been developed and sufficiently tested to show that the fundamental concept is still sound and potentially viable for the intended application. Significantly, workable solutions and approaches appear to be available for resolving questions that directly concern the C/I application (as outlined below).

Major accomplishments of the study include:

- Development and extensive testing against both analytically specified data and computed EM spectra of the frequency-domain-Prony technique.
- Extension of the above for application to magnitude-only data.
- Development and application of a frequency-domain-predictor correlator for C/I.
- Demonstration that iteratively processed data permits more accurate determination of real poles as well as separation of curve fitting and noise poles (Appendix A).

Significant results, observations and conclusions include:

- Up to 20 pole pairs can be extracted from spectral data.
- Valid poles can be obtained from band-limited-type data.
- Frequency-domain Prony is useful for interpolating discretely sampled data.
- A fairly wide, dynamic range in residue amplitude ($\geq 10^3$:1) and damping constant ($\geq$10:1) can be handled.
- Near- and far-radiated fields, scattered fields, and surface current and charge can be used to extract the poles.
- Comparison of measured and predicted results indicates the most useful frequencies for discriminating between targets.
- When a predictor-correlator approach is used, direct pole extraction is not necessary, However, it might be preferable when only a few poles are being excited for any angle of incidence.

Recommendations

We recommend the following areas for further study:

- Continue evaluation of frequency-domain-Prony pole extraction as it is affected by noise, source variations, band limited data, etc.
- Continue evaluation of predictor-correlator strategies.

- Study the information content of scattered data from the viewpoint of optimizing discriminability among targets of a given set.
- Examine the utility of pole-set data and the predictor-correlator for developing a similarity index between targets.
- Test the pole extraction procedure against experimental data by using the iterative moving-window scheme.
- Investigate the possibility for determining the information rank of spectral data and how that might be used to make C/I more effective.
- Compare the use of poles in a predictor-correlator sense as was done here, or alternatively by extracting poles from measured data for direct comparison with a library pole set via, for example, an optical correlator.
- Quantify the information content of frequency, transient and angular data.*
- Examine the feasibility for direct inversion of pattern data by using a modified-Prony technique to determine radiating source locations in space.

In closing, it is worthwhile to comment generally on target C/I and particularly on pole-descriptions in terms of their relationship to information theory. First, let us consider information in a more general way than it is in communications theory, as "knowledge acquired from data."[7] How the data is processed to develop that information and how the information is subsequently used provide the crux of the C/I problem.

We have seen that EM spectrum or waveform can be analytically expressed in simple terms of poles and residues. It may be conjectured, indeed, that the pole-residue description represents the irreducible, minimum-parameter description of the spectrum or waveform, and hence the EM characteristics of the object to which they belong. In this sense, it is interesting to speculate that a given spectrum or waveform possesses a rank or dimensionality associated with the number of parameters involved in the pole-residue description. If this is true, and the rank or the equivalent information content of the data under consideration can be established,[8,9] the implications for the C/I problem could be profound. For example, the

*Information content might be quantitatively defined as the data-rank times the number of parameters-per-rank times the number of bits-per-parameters, for a specified pole set. For sampled data, we might use the number of nonredundant input samples times the number of bits known-per-sample.

EM rank of the data would determine how many poles and residues it contains, or how many features it could yield in a more classical approach.[10] In either case, its EM rank imposes an upper limit on the information that can be extracted from the data. As we have seen, noise can reduce the rank of the data, as demonstrated by the decrease in number of poles that can be extracted from it.

However, if the problem is one of imaging rather than merely C/I, the EM rank must then equal or exceed the object's geometrical rank for the goal to achieve an image that is congruent with the actual geometry. Without restrictions on the geometry, the required information may be unavailable from finite data, i.e., the inverse problem could not be uniquely solved,[11] but the EM and geometrical ranks should not generally be expected to be equal. In any case, we intuitively expect that if C/I is the goal as opposed to imaging, the information needs should be less demanding. In other words, if we have some idea of what we're looking for, the set of objects of concern and the required information are reduced.

Thus, the concept of information content in data would seem to be a central one in C/I. The pole-residue description provides a characterization that is interpretable in an information-content sense, analytically convenient, which is why it is especially useful, besides being physically meaningful. Because the information of the time-and frequency-domains is exactly equivalent, they should be viewed as complimentary expressions. The coice of one or the other should depend on the best method for acquiring and processing the data.

Because most data available to use in the real world are obtained in the frequency domain, transient waveforms can be usually obtained only by transforming frequency-domain data.* This fact alone favors the frequency-domain technique for subsequent processing. In addition, the frequency-domain method for prediction and correlation is straightforward and makes it possible to quantitatively determine frequency intervals most useful for C/I.

In summary, we have 1) developed and validated a technique for frequency-domain pole extraction; 2) demonstrated an iterative procedure for reducing both the pole-set ambiguity due to noise and parameter variations; and 3) shown the potential of a frequency-domain predictor-correlator for C/I. Much work remains, but progress to date provides justification to continue.

---

*At best, the transform to the time domain can only preserve the information content, and may actually decrease it.

Acknowledgment

This work was supported in part by the Engineering Research Division of the Lawrence Livermore Laboratory's Electronics Engineering Department and by the Advanced Research Projects Agency.

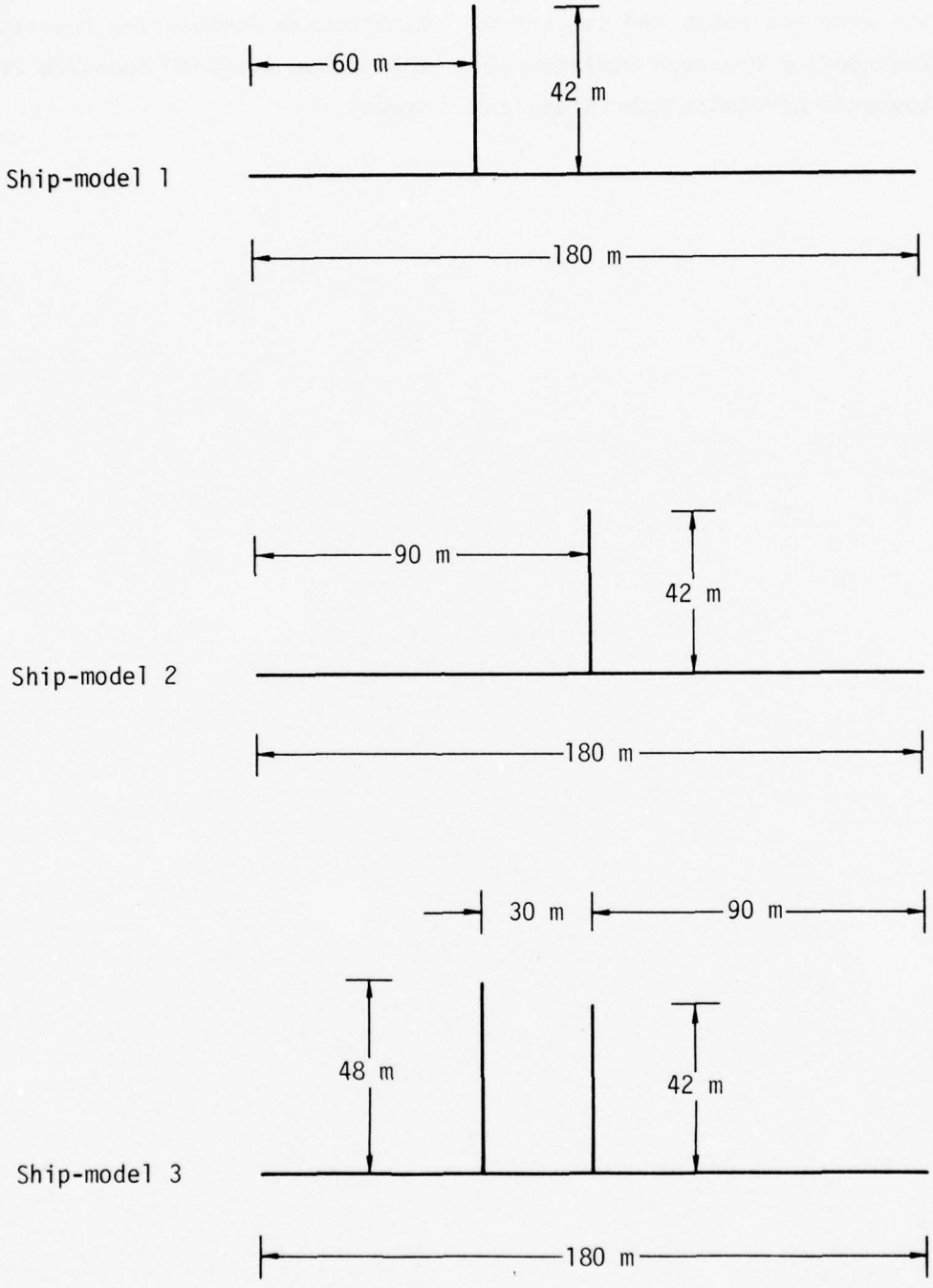

Fig. 1. Stylized ship models used to test the identification routines.

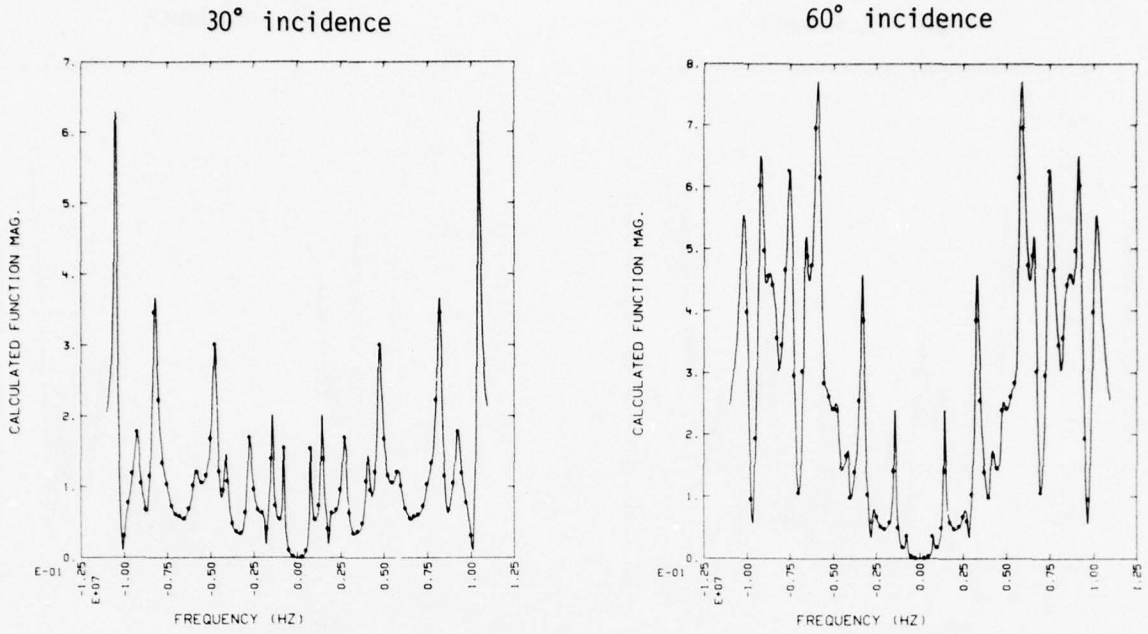

Fig. 2a. Backscattering spectra of ship-model 1 for 30° and 60° incidence.

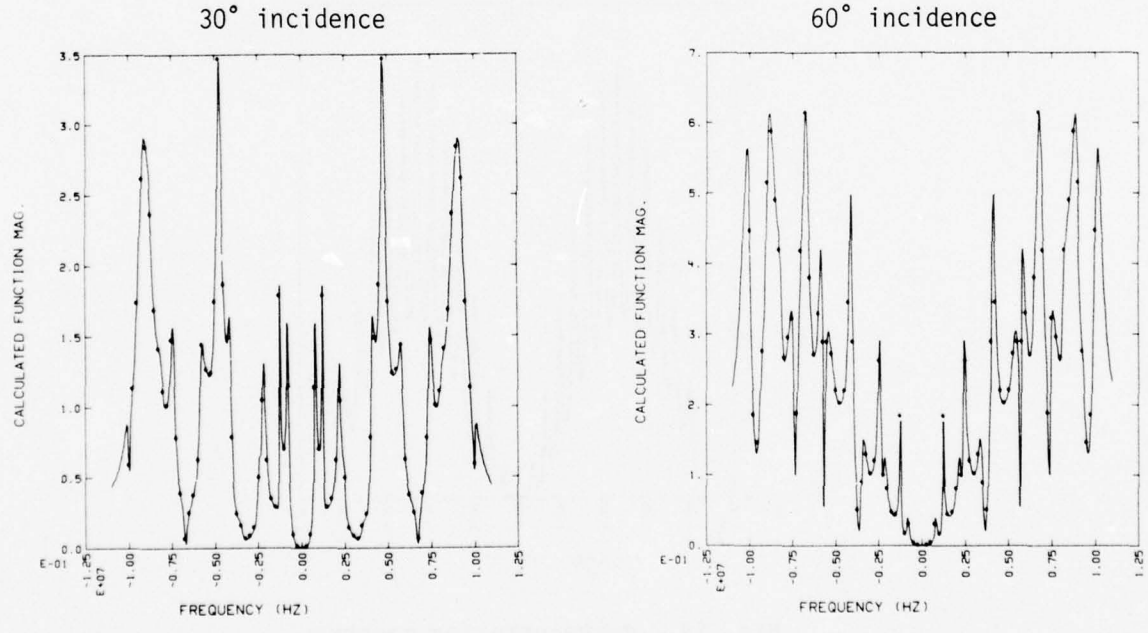

Fig. 2b. Backscattering spectra of ship-model 2 for 30° and 60° incidence.

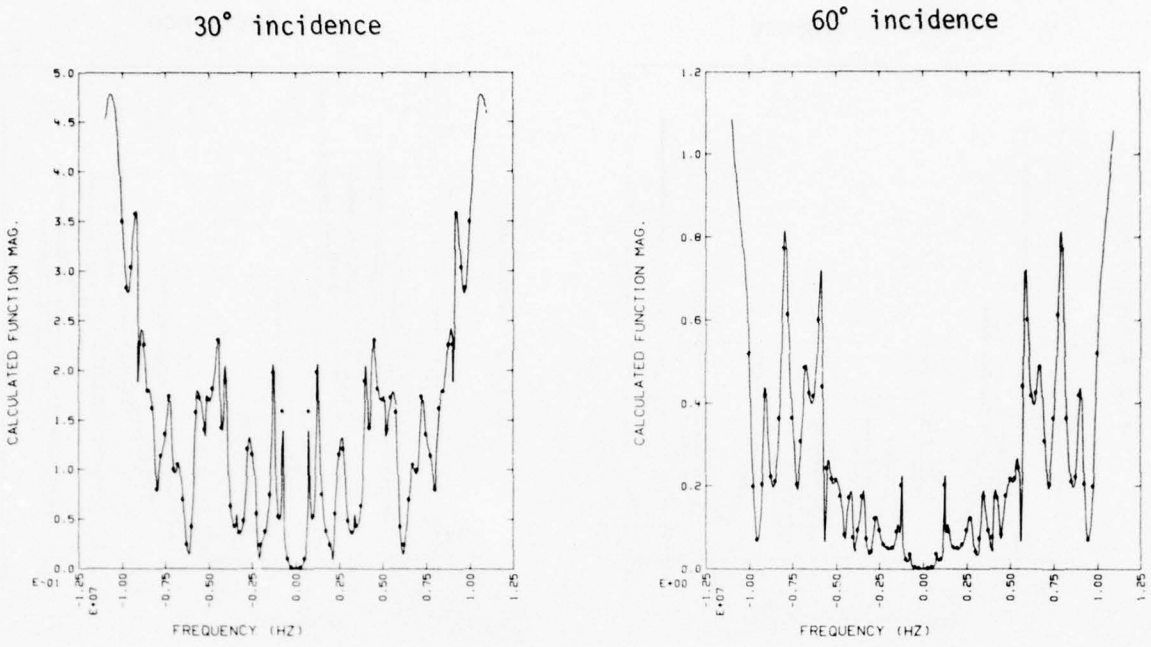

Fig. 2c. Backscattering spectra of ship-model 3 for 30° and 60° incidence.

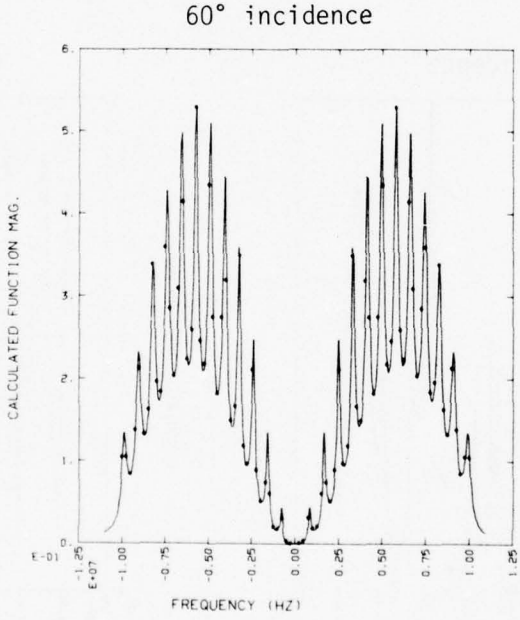

Fig. 2d. Backscattering spectra of a 180-meter wire for 60° incidence.

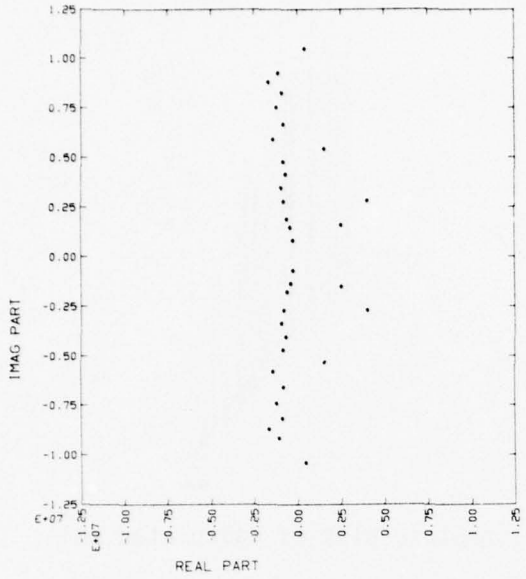

Calculated pole positions

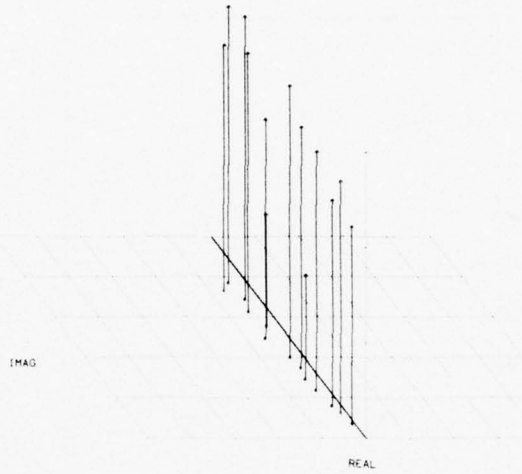

Isometric plot of calculated poles

Pole data

	REAL PART	IMAG PART
1	-2.439901E+05	7.577863E+05
2	-2.439906E+05	-7.577860E+05
3	-3.862349E+05	1.422568E+06
4	-3.862349E+05	-1.422568E+06
5	-5.708044E+05	1.832018E+06
6	-5.708044E+05	-1.832018E+06
7	-7.906113E+05	2.745295E+06
8	-7.906126E+05	-2.745295E+06
9	-9.093812E+05	3.417007E+06
10	-9.093812E+05	-3.417007E+06
11	-6.573882E+05	4.109061E+06
12	-6.573882E+05	-4.109061E+06
13	-8.303763E+05	4.740058E+06
14	-8.303763E+05	-4.740058E+06
15	-1.384734E+06	5.862336E+06
16	-1.384734E+06	-5.862336E+06
17	-7.998944E+05	6.624666E+06
18	-7.998938E+05	-6.624666E+06
19	-4.585933E+07	6.911768E+06
20	-4.585933E+07	-6.911768E+06
21	-1.415697E+07	7.133831E+06
22	-1.415697E+07	-7.133831E+06
23	-1.204921E+06	7.458264E+06
24	-1.204923E+06	-7.458264E+06
25	-8.525659E+05	8.215536E+06
26	-8.525655E+05	-8.215536E+06
27	-1.622730E+06	8.752100E+06
28	-1.622730E+06	-8.752100E+06
29	-1.058140E+06	9.200027E+06
30	-1.058140E+06	-9.200027E+06
CURVE FITTING VALUES		
31	1.553520E+06	-5.383531E+06
32	1.553520E+06	5.383531E+06
33	4.015615E+06	2.767834E+06
34	2.528214E+06	1.550119E+06
35	1.270026E+07	5.981096E+06
36	1.270026E+07	-5.981096E+06
37	4.015615E+06	-2.767834E+06
38	2.528214E+06	-1.550119E+06
39	4.713470E+05	1.045222E+07
40	4.713470E+05	-1.045222E+07

Residue data

	REAL PART	IMAG PART
1	9.195983E+02	-6.233203E+03
2	9.195849E+02	6.233173E+03
3	7.582152E+03	1.231411E+04
4	7.582117E+03	-1.231414E+04
5	-6.611710E+03	3.985701E+03
6	-6.611736E+03	-3.985644E+03
7	1.374118E+04	-1.054408E+04
8	1.374116E+04	1.054413E+04
9	6.580647E+02	1.231686E+02
10	6.580689E+02	-1.231636E+02
11	3.921140E+03	-1.767496E+04
12	3.921143E+03	1.767496E+04
13	1.612364E+04	3.496729E+04
14	1.612365E+04	-3.496730E+04
15	1.076965E+04	6.718111E+02
16	1.076964E+04	-6.717805E+02
17	-7.412509E+02	2.833903E+02
18	-7.412432E+02	-2.833783E+02
19	-7.008504E+05	-2.178638E+05
20	-7.008454E+05	2.178673E+05
21	7.268258E+04	-7.262621E+04
22	7.268188E+04	7.262475E+04
23	2.296001E+04	-1.630048E+04
24	2.295995E+04	1.630047E+04
25	-2.129168E+04	4.603790E+04
26	-2.129186E+04	-4.603792E+04
27	-2.039499E+04	-1.328282E+01
28	-2.039509E+04	1.643434E+01
29	1.245547E+04	-4.146284E+04
30	1.245547E+04	4.146289E+04
CURVE FITTING VALUES		
31	-9.240704E+01	2.094170E+02
32	-9.241648E+01	-2.094359E+02
33	-5.970479E+03	4.168002E+02
34	-1.801745E+03	7.076638E+03
35	-1.551928E+05	-1.063528E+05
36	-1.551928E+05	1.063531E+05
37	-5.970463E+03	-4.167910E+02
38	-1.801689E+03	-7.076618E+03
39	-3.276022E+04	-3.568619E+04
40	-3.276028E+04	3.568615E+04

Fig. 3a. This series of figures shows the poles and residues set found when the frequency-domain Prony is applied to the backscattering data for the ship-models shown in Fig. 1 and spectra shown in Fig. 2. The data are presented in three separate formats: 1) a Cartesian plot of all left-hand plane poles; 2) an isometric plot of the "good" poles in the second quadrant; and 3) tabulation of the poles and residues. The data shown here are for ship-model 1 at 30° incidence.

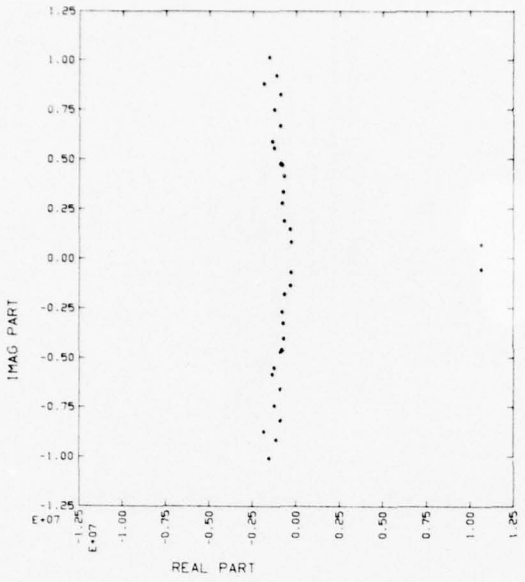

Calculated pole positions

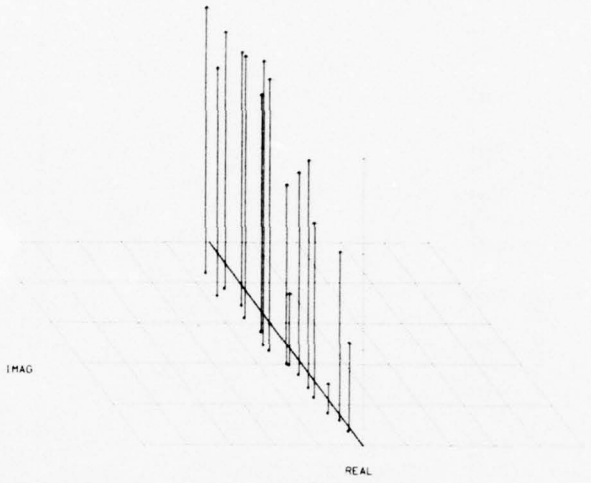

Isometric plot of calculated poles

Pole data

	REAL PART	IMAG PART
1	-2.496085E+05	7.576088E+05
2	-2.496085E+05	-7.576088E+05
3	-2.882031E+05	1.423650E+06
4	-2.882031E+05	-1.423650E+06
5	-6.305400E+05	1.846886E+06
6	-6.305397E+05	-1.846886E+06
7	-7.608380E+05	2.746950E+06
8	-7.608380E+05	-2.746950E+06
9	-8.721898E+05	3.307597E+06
10	-8.721890E+05	-3.307597E+06
11	-8.538960E+05	4.107602E+06
12	-8.538960E+05	-4.107602E+06
13	-7.664365E+05	4.656208E+06
14	-7.664410E+05	-4.656208E+06
15	-8.604434E+05	4.737480E+06
16	-8.604474E+05	-4.737479E+06
17	-1.246887E+06	5.543186E+06
18	-1.246890E+06	-5.543185E+06
19	-1.329073E+06	5.871927E+06
20	-1.329075E+06	-5.871927E+06
21	-8.896483E+05	6.639272E+06
22	-8.896512E+05	-6.639272E+06
23	-1.210077E+06	7.459281E+06
24	-1.210078E+06	-7.459282E+06
25	-8.607334E+05	8.215784E+06
26	-8.607336E+05	-8.215784E+06
27	-1.799186E+06	8.776052E+06
28	-1.799185E+06	-8.776052E+06
29	-1.079764E+06	9.207489E+06
30	-1.079765E+06	-9.207489E+06
31	-1.500978E+06	1.011381E+07
32	-1.500978E+06	-1.011381E+07
CURVE FITTING VALUES		
33	1.270873E+07	3.934021E+06
34	1.270873E+07	-3.934021E+06
35	1.560874E+07	6.307575E+06
36	1.560874E+07	-6.307575E+06
37	1.067620E+07	6.233317E+05
38	1.067620E+07	-6.233317E+05
39	1.415920E+07	9.283330E+06
40	1.415920E+07	-9.283330E+06

Residue data

	REAL PART	IMAG PART
1	-4.029004E+01	-1.543135E+03
2	-4.029396E+01	1.543128E+03
3	2.607074E+03	1.021608E+04
4	2.607057E+03	-1.021609E+04
5	3.621913E+02	7.330239E+01
6	3.621695E+02	-7.330086E+01
7	1.164880E+04	-3.929885E+03
8	1.164879E+04	3.929837E+03
9	-2.467624E+04	3.682854E+04
10	-2.467629E+04	-3.682842E+04
11	4.168221E+03	-2.351869E+04
12	4.168325E+03	2.351880E+04
13	6.502027E+02	7.899485E+02
14	6.515882E+02	-7.894848E+02
15	-7.555451E+03	-1.140232E+04
16	-7.556934E+03	1.140147E+04
17	1.303487E+04	1.279878E+05
18	1.303423E+04	-1.279883E+05
19	-4.908576E+04	-1.670120E+05
20	-4.908525E+04	1.670130E+05
21	-5.172008E+04	2.190701E+04
22	-5.172032E+04	-2.190691E+04
23	9.808592E+04	-3.025644E+04
24	9.808572E+04	3.025628E+04
25	-6.863641E+04	4.683044E+04
26	-6.863635E+04	-4.683166E+04
27	3.073167E+04	-3.271788E+04
28	3.072937E+04	3.271834E+04
29	8.744126E+04	-2.298097E+04
30	8.744153E+04	2.298204E+04
31	-6.471335E+04	9.388823E+04
32	-6.471415E+04	-9.388654E+04
CURVE FITTING VALUES		
33	1.846642E+05	-2.158323E+05
34	1.846654E+05	2.158382E+05
35	8.821144E+05	1.348089E+05
36	8.821059E+05	-1.348096E+05
37	1.143251E+05	1.905225E+04
38	1.143271E+05	-1.904958E+04
39	-8.156054E+05	8.546496E+05
40	-8.156024E+05	-8.546465E+05

Fig. 3b. Same as Fig. 3a, except for ship-model 1 at 60° incidence.

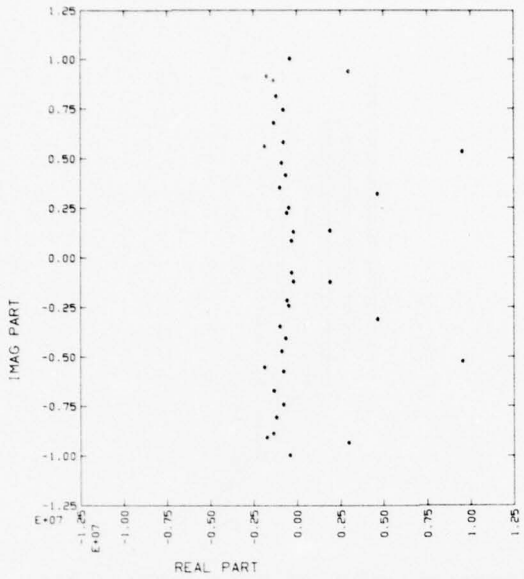

Calculated pole positions

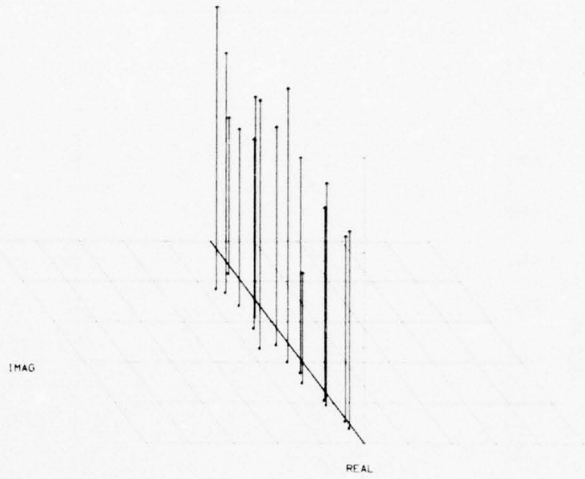

Isometric plot of calculated poles

Pole data

	REAL PART	IMAG PART
1	-2.664562E+05	7.887394E+05
2	-2.664525E+05	-7.887386E+05
3	-1.626363E+05	1.245997E+06
4	-1.626343E+05	-1.245997E+06
5	-5.447921E+05	2.184356E+06
6	-5.447919E+05	-2.184356E+06
7	-4.445694E+05	2.460318E+06
8	-4.445681E+05	-2.460318E+06
9	-9.452684E+05	3.488792E+06
10	-9.452684E+05	-3.488792E+06
11	-6.165755E+05	4.103687E+06
12	-6.165755E+05	-4.103687E+06
13	-8.661994E+05	4.742659E+06
14	-8.661991E+05	-4.742659E+06
15	-1.834990E+06	5.553614E+06
16	-1.834991E+06	-5.553614E+06
17	-7.699373E+05	5.763795E+06
18	-7.699354E+05	-5.763795E+06
19	-1.294269E+06	6.751635E+06
20	-1.294268E+06	-6.751634E+06
21	-7.710999E+05	7.421621E+06
22	-7.710986E+05	-7.421620E+06
23	-1.160624E+06	8.102527E+06
24	-1.160620E+06	-8.102527E+06
25	-1.342777E+06	8.895848E+06
26	-1.342791E+06	-8.895847E+06
27	-1.706781E+06	9.108648E+06
28	-1.706777E+06	-9.108648E+06
29	-3.818148E+05	1.000660E+07
30	-3.818150E+05	-1.000660E+07
CURVE FITTING VALUES		
31	9.579095E+06	5.291170E+06
32	9.579095E+06	-5.291170E+06
33	4.684404E+06	-3.158113E+06
34	4.684404E+06	3.158113E+06
35	1.921115E+06	-1.297709E+06
36	1.921115E+06	1.297709E+06
37	1.476491E+07	-7.280426E+06
38	1.476491E+07	7.280426E+06
39	3.012857E+06	9.360178E+06
40	3.012857E+06	-9.360178E+06

Residue data

	REAL PART	IMAG PART
1	1.836119E+03	-7.155130E+03
2	1.836099E+03	7.155029E+03
3	5.963571E+02	5.409420E+03
4	5.963710E+02	-5.409436E+03
5	-1.156735E+04	6.773291E+03
6	-1.156733E+04	-6.773279E+03
7	1.504401E+03	-6.478364E+03
8	1.504413E+03	6.478367E+03
9	4.357499E+02	-7.789987E+02
10	4.357539E+02	7.790044E+02
11	2.507009E+03	-1.115926E+04
12	2.507016E+03	1.115927E+04
13	-4.123058E+04	2.326129E+04
14	-4.123056E+04	-2.326126E+04
15	2.250582E+04	-1.213313E+04
16	2.250592E+04	1.213323E+04
17	3.495617E+03	-1.173137E+04
18	3.495613E+03	1.173132E+04
19	3.564459E+03	4.906915E+03
20	3.564526E+03	-4.906912E+03
21	3.140875E+03	-1.254318E+04
22	3.140930E+03	1.254303E+04
23	1.934557E+03	-4.057689E+03
24	1.934485E+03	4.057997E+03
25	-2.055165E+04	-1.954783E+03
26	-2.055013E+04	1.956458E+03
27	-4.872893E+04	-3.269911E+04
28	-4.872986E+04	3.269651E+04
29	1.491088E+03	-2.278329E+03
30	1.491044E+03	2.277733E+03
CURVE FITTING VALUES		
31	-1.655711E+04	4.344691E+04
32	-1.655665E+04	-4.344585E+04
33	-2.603954E+03	5.640934E+03
34	-2.603980E+03	-5.640738E+03
35	2.506337E+03	-2.404816E+03
36	2.506245E+03	2.405004E+03
37	1.366876E+05	9.443970E+02
38	1.366910E+05	-9.443722E+02
39	5.310088E+03	-3.535390E+03
40	5.310257E+03	3.533939E+03

Fig. 3c. Same as Fig. 3a, except for ship-model 2 at 30° incidence.

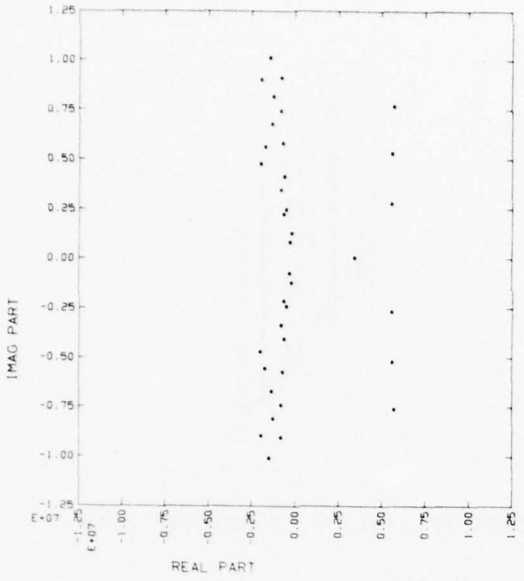

Calculated pole positions

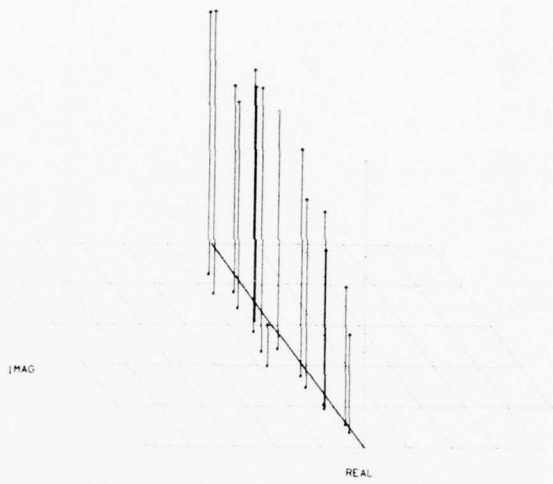

Isometric plot of calculated poles

Pole data

	REAL PART	IMAG PART
1	-2.891012E+05	7.884878E+05
2	-2.891012E+05	-7.884878E+05
3	-1.753438E+05	1.253063E+06
4	-1.753438E+05	-1.253063E+06
5	-6.551896E+05	2.184576E+06
6	-6.551902E+05	-2.184576E+06
7	-5.033732E+05	2.442225E+06
8	-5.033732E+05	-2.442225E+06
9	-8.022914E+05	3.418982E+06
10	-8.022914E+05	-3.418982E+06
11	-6.198677E+05	4.100003E+06
12	-6.198677E+05	-4.100003E+06
13	-1.980139E+06	4.743244E+06
14	-1.980139E+06	-4.743244E+06
15	-1.718544E+06	5.582944E+06
16	-1.718544E+06	-5.582944E+06
17	-6.990619E+05	5.759074E+06
18	-6.990601E+05	-5.759074E+06
19	-1.334663E+06	6.748002E+06
20	-1.334664E+06	-6.748002E+06
21	-7.762277E+05	7.419986E+06
22	-7.762287E+05	-7.419986E+06
23	-1.236213E+06	8.120527E+06
24	-1.236211E+06	-8.120527E+06
25	-1.953936E+06	8.982524E+06
26	-1.953936E+06	-8.982524E+06
27	-7.962534E+05	9.074394E+06
28	-7.962536E+05	-9.074394E+06
29	-1.454137E+06	1.010778E+07
30	-1.454137E+06	-1.010778E+07
CURVE FITTING VALUES		
31	5.623887E+06	5.266650E+06
32	5.623887E+06	-5.266650E+06
33	5.558008E+06	-2.723862E+06
34	5.558008E+06	2.723862E+06
35	3.460340E+06	-6.094598E-04
36	5.741116E+06	-7.642442E+06
37	-1.768498E+07	1.536285E-09
38	5.741116E+06	7.642442E+06
39	1.061750E+08	3.407560E+06
40	1.061750E+08	-3.407560E+06

Residue data

	REAL PART	IMAG PART
1	5.707134E+02	-1.978406E+03
2	5.707173E+02	1.978404E+03
3	4.224318E+03	3.288776E+03
4	4.224321E+03	-3.288779E+03
5	-2.453044E+03	-8.455533E+03
6	-2.453036E+03	8.455556E+03
7	5.075494E+03	-1.952360E+04
8	5.075510E+03	1.952358E+04
9	-1.746748E+04	4.262389E+03
10	-1.746748E+04	-4.262376E+03
11	1.250301E+04	-4.393301E+04
12	1.250302E+04	4.393303E+04
13	-5.161592E+02	2.087294E+01
14	-5.161527E+02	-2.080211E+01
15	-1.029308E+05	4.682871E+04
16	-1.029308E+05	-4.682834E+04
17	1.932835E+04	-5.672405E+04
18	1.932851E+04	5.672386E+04
19	-1.084827E+05	1.008297E+04
20	-1.084825E+05	-1.008285E+04
21	2.021752E+04	-5.130159E+04
22	2.021761E+04	5.130164E+04
23	4.369828E+03	-2.808562E+04
24	4.369799E+03	2.808587E+04
25	-5.758131E+04	1.725414E+05
26	-5.757990E+04	-1.725413E+05
27	1.670015E+04	-2.329581E+04
28	1.669955E+04	2.329555E+04
29	-1.084339E+05	3.023017E+04
30	-1.084332E+05	-3.023041E+04
CURVE FITTING VALUES		
31	-6.060536E+03	-1.628993E+03
32	-6.060518E+03	1.629358E+03
33	1.745120E+03	-4.317458E+03
34	1.745207E+03	4.317505E+03
35	-4.706399E+02	-1.302645E-02
36	2.242426E+03	5.918764E+03
37	4.345325E+03	6.611859E-02
38	2.242883E+03	-5.918040E+03
39	1.387348E+06	-5.912724E+06
40	1.387474E+06	5.912696E+06

Fig. 3d. Same as Fig. 3a, except for ship-model 2 at 60° incidence.

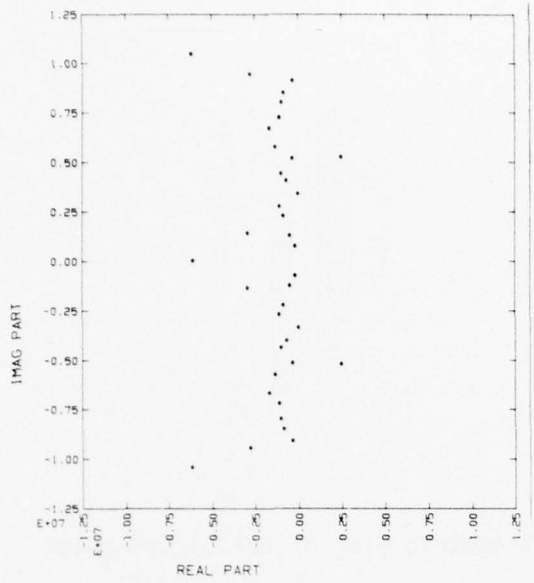

Calculated pole positions

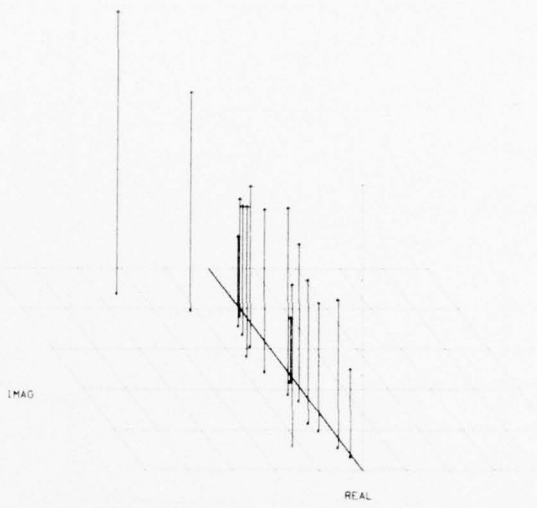

Isometric plot of calculated poles

Pole data

	REAL PART	IMAG PART
1	1.454907E+03	-4.325577E+03
2	1.454917E+03	4.325538E+03
3	1.198934E+04	1.557811E+04
4	1.198894E+04	-1.557879E+04
5	-2.362686E+04	-1.290400E+04
6	-2.362680E+04	1.290538E+04
7	-8.404129E+03	8.855552E+03
8	-8.404015E+03	-8.855433E+03
9	6.982211E+03	-1.607936E+04
10	6.982549E+03	1.607933E+04
11	2.154680E+04	-1.196295E+04
12	2.154687E+04	1.196300E+04
13	-2.183792E+04	4.588214E+04
14	-2.183784E+04	-4.588217E+04
15	-8.512182E+02	-2.449207E+03
16	-8.511767E+02	2.449204E+03
17	7.070246E+03	-2.726539E+04
18	7.070345E+03	2.726539E+04
19	1.214789E+04	1.672391E+04
20	1.214799E+04	-1.672391E+04
21	2.524640E+04	9.556323E+03
22	2.524650E+04	-9.556364E+03
23	2.042783E+03	1.204352E+04
24	2.042858E+03	-1.204344E+04
25	-2.221314E+03	4.269602E+03
26	-2.221091E+03	-4.269785E+03
27	9.305155E+03	3.586637E+02
28	9.305283E+03	-3.567855E+02
29	-8.331093E+04	6.994281E+04
30	-8.331081E+04	-6.994318E+04
31	-4.143714E+05	-3.098460E+05
32	-4.143722E+05	3.098455E+05
CURVE FITTING VALUES		
33	-4.075776E+03	3.762830E+03
34	-4.075808E+03	-3.762729E+03
35	5.987199E+02	2.879268E+01
36	5.987452E+02	-2.879342E+01
37	3.279235E+04	-2.509140E+05
38	3.279178E+04	2.509141E+05
39	-2.602984E+04	-2.344120E-01
40	1.422711E+05	2.901771E-01

Residue data

	REAL PART	IMAG PART
1	-1.824622E+05	7.434225E+05
2	-1.824626E+05	-7.434225E+05
3	-4.759116E+05	1.270015E+06
4	-4.759188E+05	-1.270013E+06
5	-2.915460E+06	1.380253E+06
6	-2.915453E+06	-1.380253E+06
7	-8.582620E+05	2.253153E+06
8	-8.582539E+05	-2.253154E+06
9	-1.105486E+06	2.729810E+06
10	-1.105492E+06	-2.729808E+06
11	-6.735660E+05	4.035273E+06
12	-6.735660E+05	-4.035273E+06
13	-9.998854E+05	4.402102E+06
14	-9.998854E+05	-4.402102E+06
15	-3.482497E+05	5.165678E+06
16	-3.482496E+05	-5.165678E+06
17	-1.341599E+06	5.755483E+06
18	-1.341599E+06	-5.755483E+06
19	-1.656095E+06	6.697465E+06
20	-1.656096E+06	-6.697465E+06
21	-1.083259E+06	7.237322E+06
22	-1.083262E+06	-7.237322E+06
23	-9.779020E+05	7.995790E+06
24	-9.779068E+05	-7.995790E+06
25	-8.587189E+05	8.493436E+06
26	-8.587171E+05	-8.493436E+06
27	-3.491563E+05	9.101757E+06
28	-3.491553E+05	-9.101757E+06
29	-2.805139E+06	9.451888E+06
30	-2.805139E+06	-9.451888E+06
31	-6.153979E+06	1.045240E+07
32	-6.153979E+06	-1.045240E+07
CURVE FITTING VALUES		
33	2.465933E+06	5.238087E+06
34	2.465933E+06	-5.238087E+06
35	8.693712E+02	3.374182E+06
36	8.695092E+02	-3.374182E+06
37	1.430245E+07	7.166093E+06
38	1.430245E+07	-7.166093E+06
39	-6.073766E+06	3.123513E-04
40	1.691990E+07	-7.894944E-05

Fig. 3e. Same as Fig. 3a, except for ship-model 3 at 30° incidence.

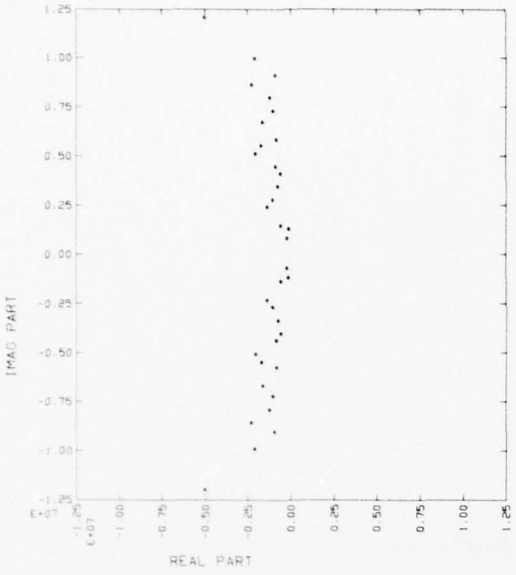

Calculated pole positions

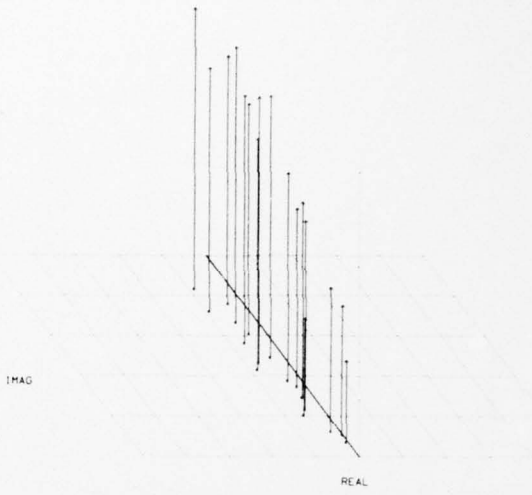

Isometric plot of calculated poles

Pole data

	REAL PART	IMAG PART
1	-2.023101E+05	7.590681E+05
2	-2.023101E+05	-7.590681E+05
3	-9.906452E+04	1.230711E+06
4	-9.906399E+04	-1.230710E+06
5	-5.801541E+05	1.420674E+06
6	-5.801512E+05	-1.420672E+06
7	-1.380992E+06	2.377084E+06
8	-1.380988E+06	-2.377084E+06
9	-1.084163E+06	2.718041E+06
10	-1.084163E+06	-2.718041E+06
11	-7.582955E+05	3.409560E+06
12	-7.582965E+05	-3.409560E+06
13	-5.958623E+05	4.059848E+06
14	-5.958624E+05	-4.059848E+06
15	-8.450507E+05	4.423966E+06
16	-8.450507E+05	-4.423966E+06
17	-2.054318E+06	5.100283E+06
18	-2.054318E+06	-5.100284E+06
19	-1.702471E+06	5.513225E+06
20	-1.702470E+06	-5.513225E+06
21	-8.323874E+05	5.802157E+06
22	-8.323859E+05	-5.802157E+06
23	-1.635117E+06	6.710259E+06
24	-1.635117E+06	-6.710259E+06
25	-1.026025E+06	7.251430E+06
26	-1.026023E+06	-7.251430E+06
27	-1.247541E+06	7.953704E+06
28	-1.247538E+06	-7.953704E+06
29	-2.270352E+06	8.597125E+06
30	-2.270353E+06	-8.597125E+06
31	-9.097504E+05	9.073615E+06
32	-9.097523E+05	-9.073615E+06
33	-2.126343E+06	9.946341E+06
34	-2.126343E+06	-9.946341E+06
CURVE FITTING VALUES		
35	1.740008E+07	2.690024E+06
36	1.430169E+07	-7.454706E+06
37	1.430169E+07	7.454706E+06
38	1.740008E+07	-2.690024E+06
39	-5.014934E+06	-1.203482E+07
40	-5.014934E+06	1.203482E+07

Residue data

	REAL PART	IMAG PART
1	-5.201974E+02	-1.244447E+03
2	-5.202021E+02	1.244444E+03
3	5.512999E+02	4.185202E+03
4	5.512707E+02	-4.185209E+03
5	4.850547E+03	3.575581E+03
6	4.850547E+03	-3.575582E+03
7	-1.572366E+03	-1.113209E+03
8	-1.572416E+03	1.113162E+03
9	1.775538E+04	2.948512E+03
10	1.775533E+04	-2.948473E+03
11	-2.133098E+04	2.161606E+03
12	-2.133100E+04	-2.161599E+03
13	-8.869493E+03	-1.103149E+04
14	-8.869504E+03	1.103144E+04
15	2.836253E+04	5.986178E+03
16	2.836245E+04	-5.986202E+03
17	-3.876604E+04	3.289690E+04
18	-3.876681E+04	-3.289714E+04
19	-1.134886E+05	-3.217525E+04
20	-1.134888E+05	3.217634E+04
21	4.551725E+04	-9.928057E+04
22	4.551775E+04	9.928034E+04
23	-6.086672E+04	-4.828477E+04
24	-6.086676E+04	4.828481E+04
25	2.253281E+04	4.486187E+04
26	2.253263E+04	-4.486174E+04
27	-9.361153E+03	-1.541541E+05
28	-9.361279E+03	1.541542E+05
29	-2.609619E+04	-6.568263E+04
30	-2.609615E+04	6.568304E+04
31	7.624555E+04	1.849097E+04
32	7.624564E+04	-1.849995E+04
33	-1.099989E+05	-1.374607E+05
34	-1.099990E+05	1.374606E+05
CURVE FITTING VALUES		
35	-6.838941E+05	-1.188626E+05
36	-2.648339E+05	1.098972E+06
37	-2.648355E+05	1.098971E+06
38	-6.838942E+05	1.188621E+05
39	9.003074E+05	-9.585729E+05
40	9.003054E+05	9.585760E+05

Fig. 3f. Same as Fig. 3a, except for ship-model 3 at 60° incidence.

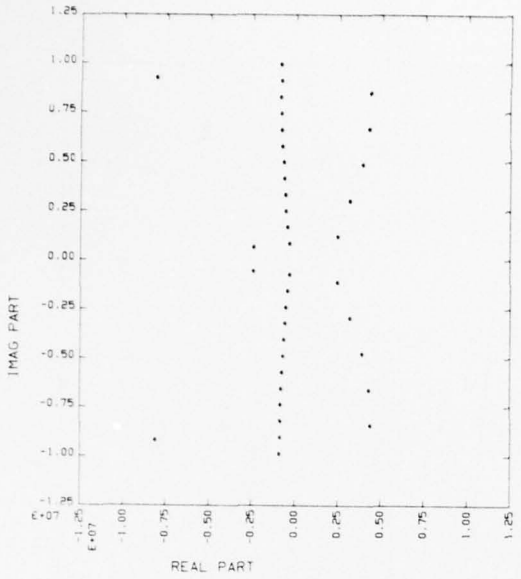

Calculated pole positions

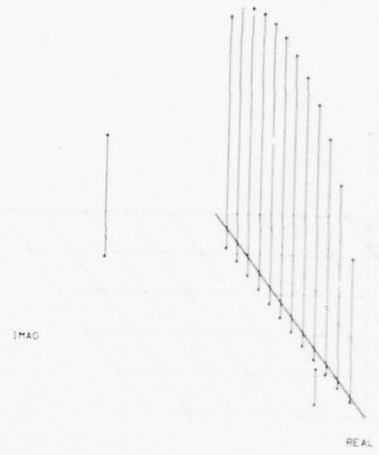

Isometric plot of calculated poles

Pole data

	REAL PART	IMAG PART
1	-2.379374E+06	6.096928E+05
2	-2.379374E+06	-6.096928E+05
3	-2.845557E+05	7.915284E+05
4	-2.845584E+05	-7.915286E+05
5	-4.166226E+05	1.615758E+06
6	-4.166226E+05	-1.615758E+06
7	-5.016540E+05	2.441824E+06
8	-5.016541E+05	-2.441824E+06
9	-5.664528E+05	3.269612E+06
10	-5.664529E+05	-3.269612E+06
11	-6.196292E+05	4.098216E+06
12	-6.196292E+05	-4.098216E+06
13	-6.658842E+05	4.927337E+06
14	-6.658843E+05	-4.927337E+06
15	-7.062526E+05	5.756869E+06
16	-7.062526E+05	-5.756869E+06
17	-7.432134E+05	6.586696E+06
18	-7.432129E+05	-6.586696E+06
19	-7.765019E+05	7.416719E+06
20	-7.765023E+05	-7.416719E+06
21	-8.073962E+05	8.246933E+06
22	-8.073973E+05	-8.246933E+06
23	-8.350733E+05	9.077290E+06
24	-8.350736E+05	-9.077290E+06
25	-8.076923E+06	9.219719E+06
26	-8.076923E+06	-9.219719E+06
27	-8.490728E+05	9.910273E+06
28	-8.490728E+05	-9.910273E+06
CURVE FITTING VALUES		
29	3.925500E+06	-4.813266E+06
30	3.925500E+06	4.813266E+06
31	3.224694E+06	2.980841E+06
32	2.519166E+06	-1.158206E+06
33	4.339738E+06	-6.647276E+06
34	4.339738E+06	6.647276E+06
35	3.224694E+06	-2.980841E+06
36	2.519166E+06	1.158206E+06
37	4.411881E+06	8.455420E+06
38	8.205798E+07	1.226558E-07
39	4.411861E+06	-8.455420E+06
40	-1.387463E+08	5.182581E-16

Residue data

	REAL PART	IMAG PART
1	-5.979992E+01	1.414636E+02
2	-5.981506E+01	-1.414772E+02
3	4.760913E+02	-2.068227E+03
4	4.761048E+02	2.068247E+03
5	-2.159969E+03	8.872745E+03
6	-2.159968E+03	-8.872746E+03
7	4.904408E+03	-1.938937E+04
8	4.904410E+03	1.938937E+04
9	-8.501741E+03	3.189653E+04
10	-8.501736E+03	-3.189654E+04
11	1.253808E+04	-4.389194E+04
12	1.253809E+04	4.389194E+04
13	-1.630000E+04	5.321844E+04
14	-1.629999E+04	-5.321845E+04
15	1.921669E+04	-5.802677E+04
16	1.921667E+04	5.802676E+04
17	-2.068050E+04	5.735413E+04
18	-2.068045E+04	-5.735414E+04
19	2.034097E+04	-5.128618E+04
20	2.034099E+04	5.128620E+04
21	-1.820387E+04	4.091466E+04
22	-1.820371E+04	-4.091466E+04
23	1.446310E+04	-2.816977E+04
24	1.446319E+04	2.816980E+04
25	7.849424E+02	9.758460E+02
26	7.841638E+02	-9.755943E+02
27	-9.333700E+03	1.584388E+04
28	-9.333630E+03	-1.584369E+04
CURVE FITTING VALUES		
29	-5.633229E+02	-1.680909E+03
30	-5.632695E+02	1.680991E+03
31	-5.820485E+02	9.195603E+02
32	-4.534184E+02	-4.013203E+02
33	-1.862979E+02	-2.345435E+03
34	-1.860416E+02	2.345656E+03
35	-5.820939E+02	-9.195443E+02
36	-4.533844E+02	4.013310E+02
37	5.600846E+02	2.444894E+03
38	-6.473863E+04	3.434922E+02
39	5.595697E+02	-2.444963E+03
40	-3.887397E+04	2.243487E+00

Fig. 3g. Same as Fig. 3a, except a 180-m wire at 60° incidence.

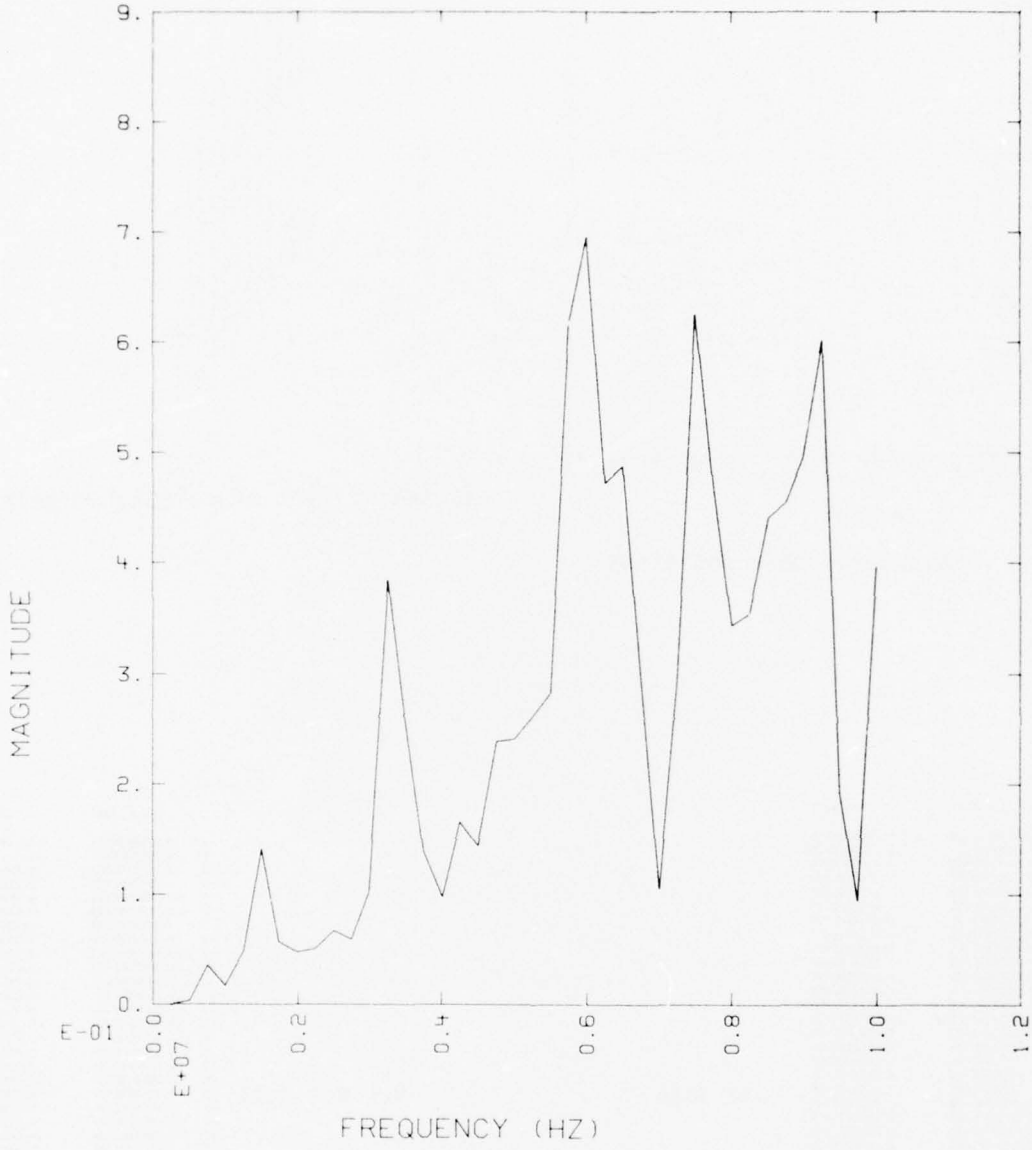

Fig. 4a. This series of figures shows the results obtained when the predictor-correlator algorithm is used to identify a scattered response by three sets of stored library poles. The backscattered data shown in this figure are for ship-model 1 at 60°. The three sets of library poles used in the identification algorithm are for ship-models 1, 2, and 3 at 60°. This figure shows the magnitude data of all points used for both the calculation of residues and the subsequent identification calculation.

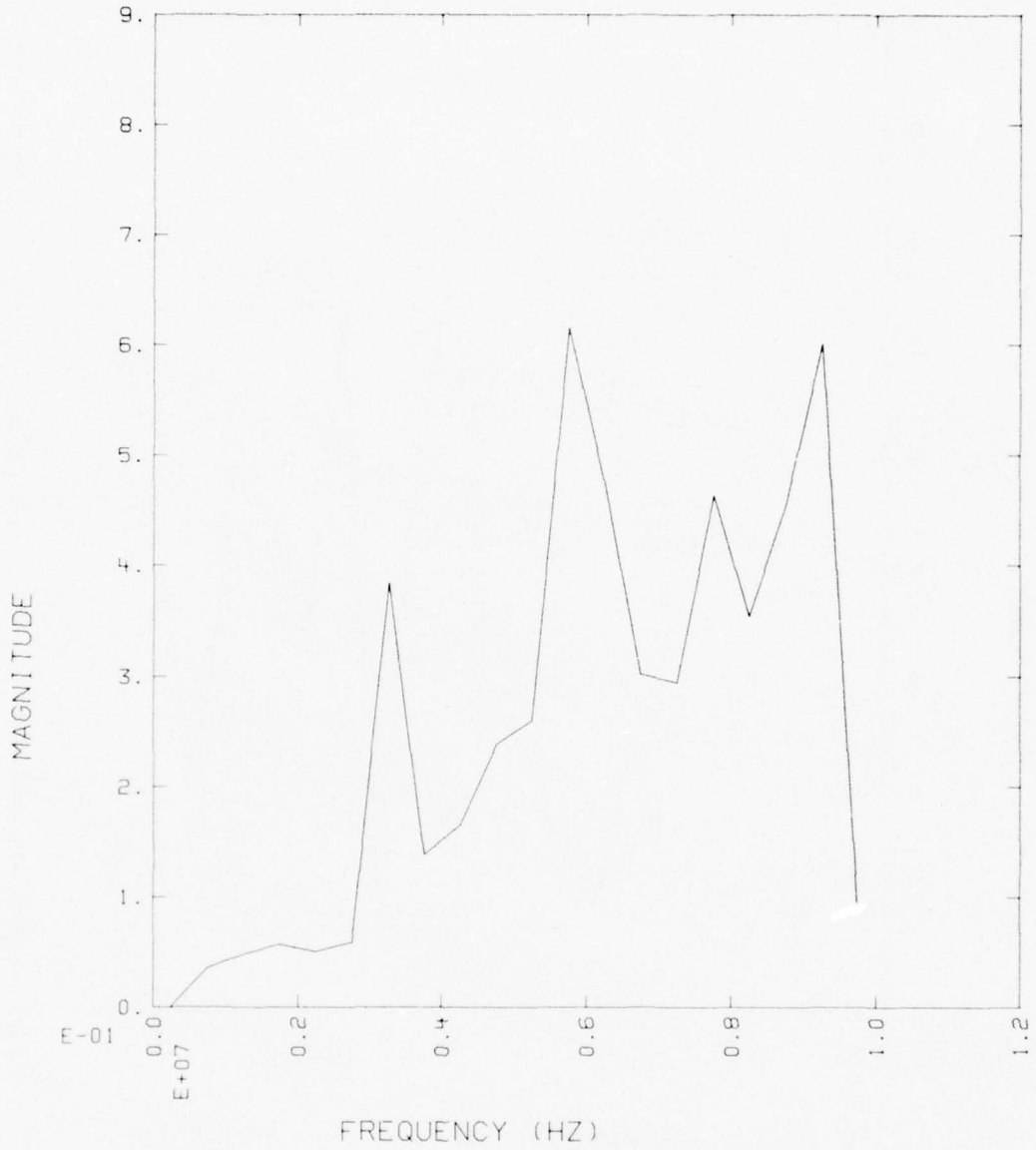

Fig. 4b. The magnitude plot of the scattered response shown in Fig. 4a for the points where the residues will be calculated is shown.

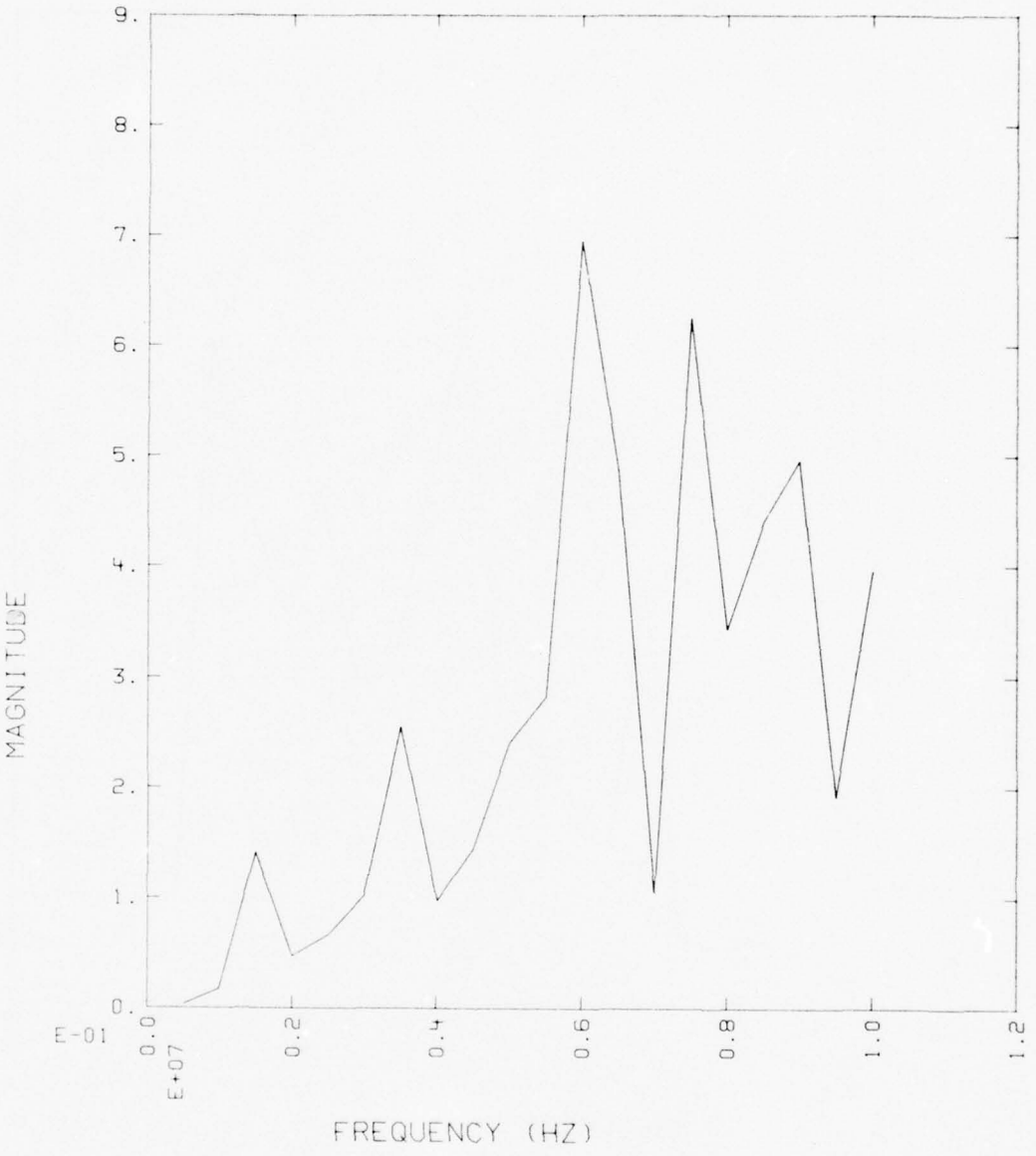

Fig. 4c. The magnitude plot of the scattered response in Fig. 4a at those points to be used for identification is shown.

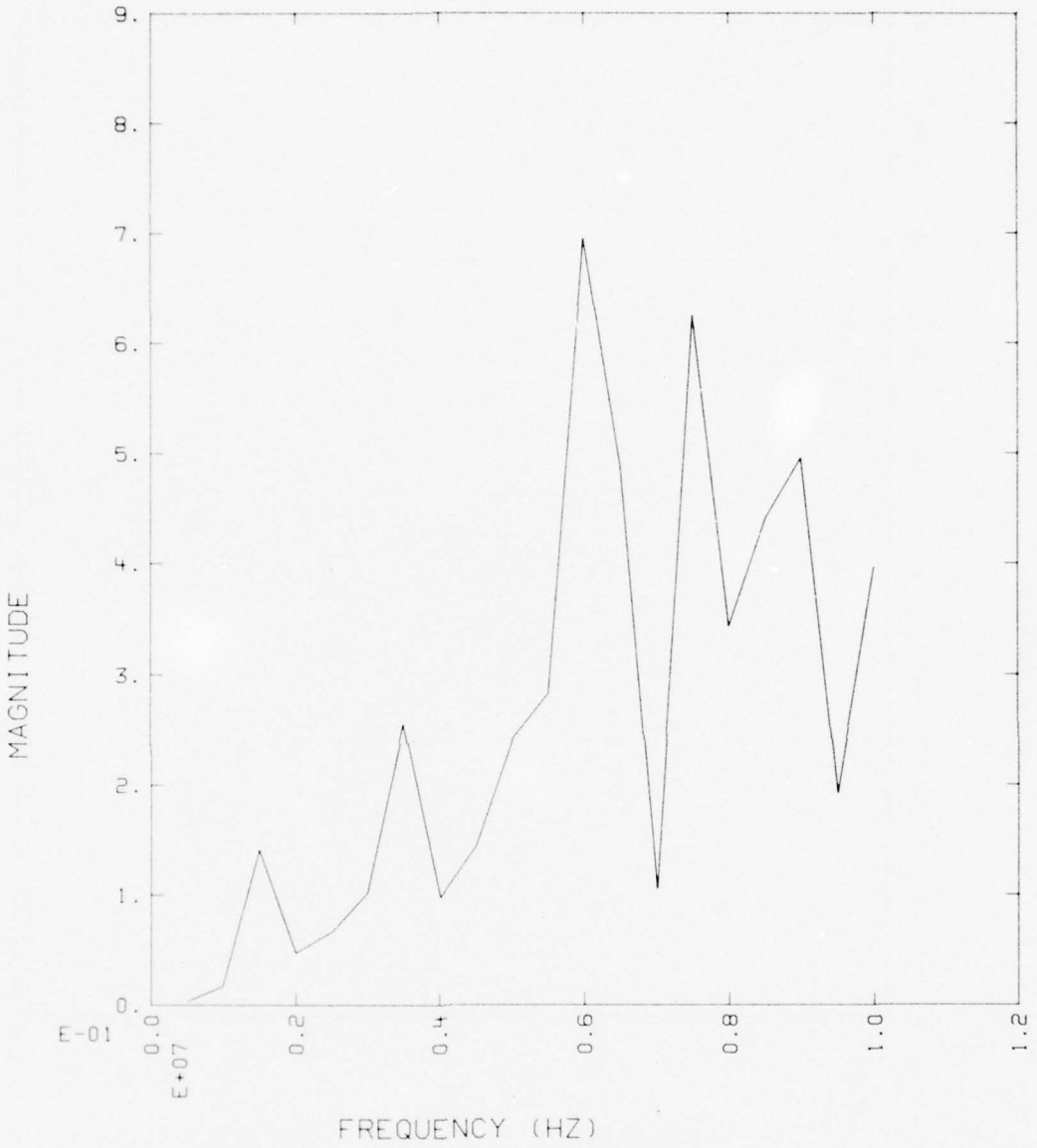

Fig. 4d. The magnitude plot of the calculated identification response for ship-model 1 is shown. This response is found by using the stored library poles for ship-model 1 and the data in Fig. 4b to calculate a set of residues. This set of residues and the stored pole set are then used to calculate a response function at the identification points.

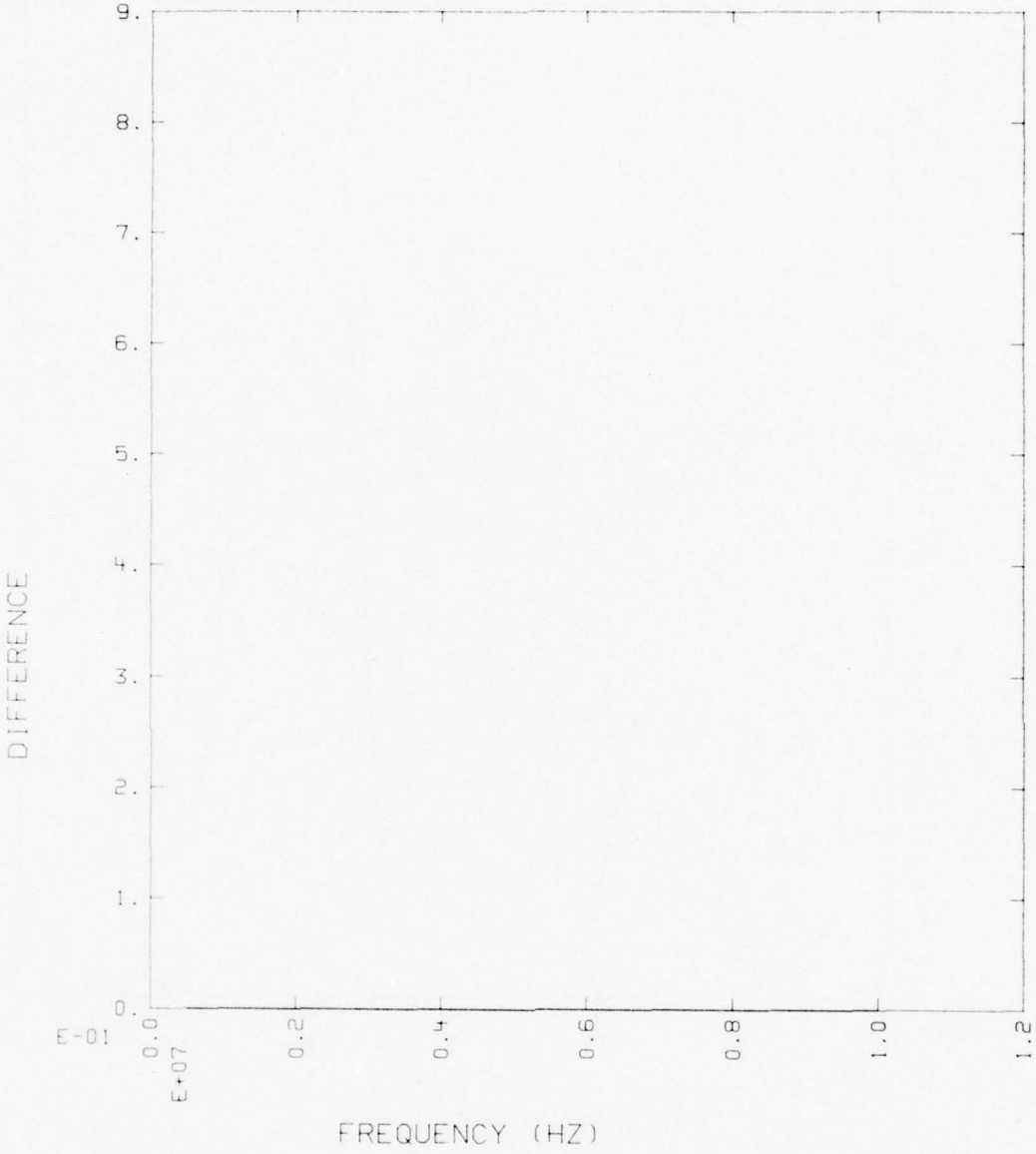

Fig. 4e. The magnitude plot of the difference between the measured and calculated responses at the identification points is shown. This function is found by subtracting the response used to find Fig. 4d from the response used to find Fig. 4c. The identification number [Eq. (4a)] with ship-model 1 is equal to 0.0.

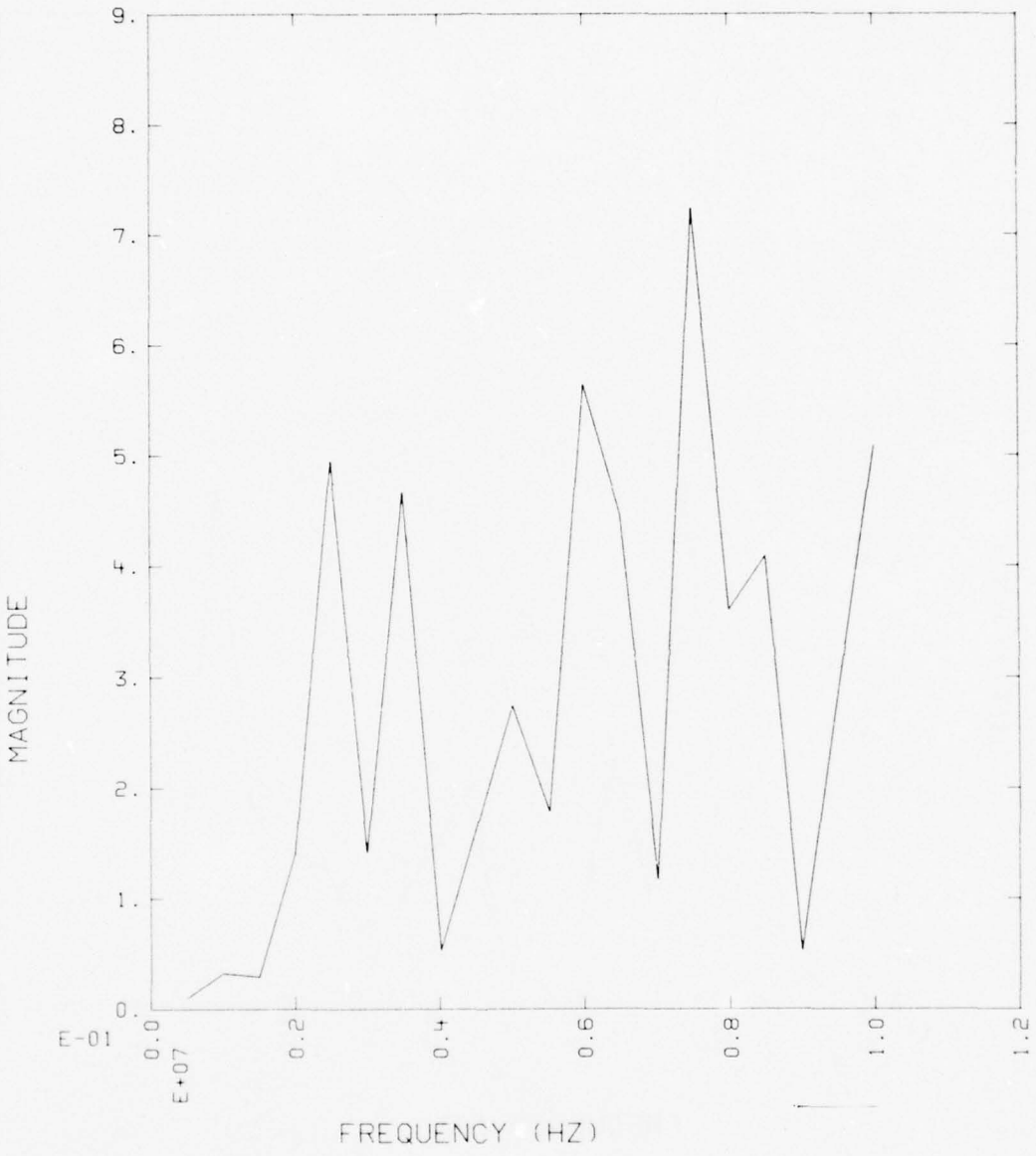

Fig. 4f. The magnitude plot of the calculated identification response for ship-model 2 is shown. This response is found by using the stored library poles for ship-model 2 and the data in Fig. 4b to calculate a set of residues. This set of residues and the stored pole set are then used to calculate a response function at the identification points.

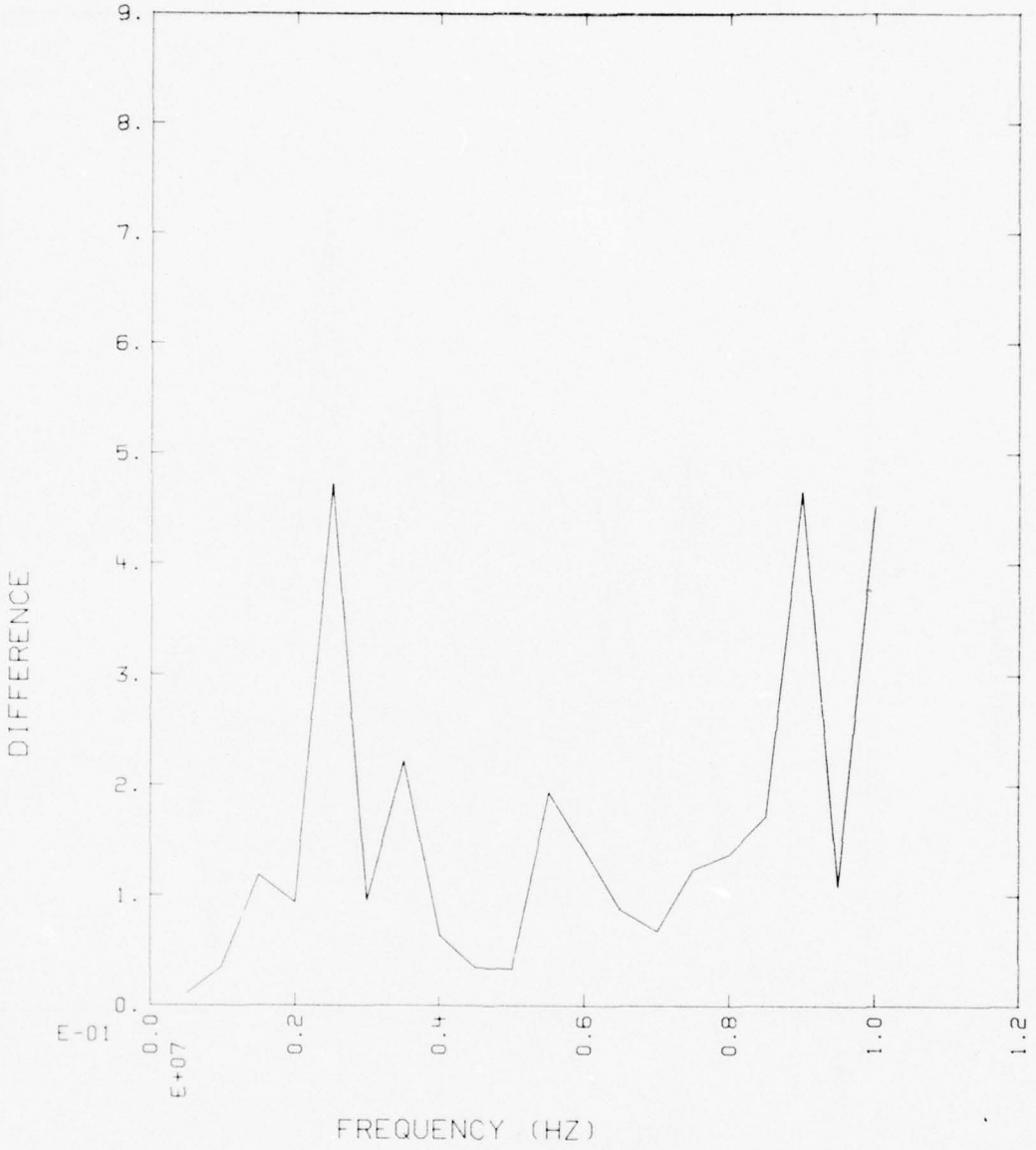

Fig. 4g. The magnitude plot of the difference between the measured and calculated responses at the identification points is shown. This function is found by subtracting the response used to find Fig. 4f from the response used to find Fig. 4c. The identification number [Eq. (4a)] with ship-model 2 is equal to 0.156.

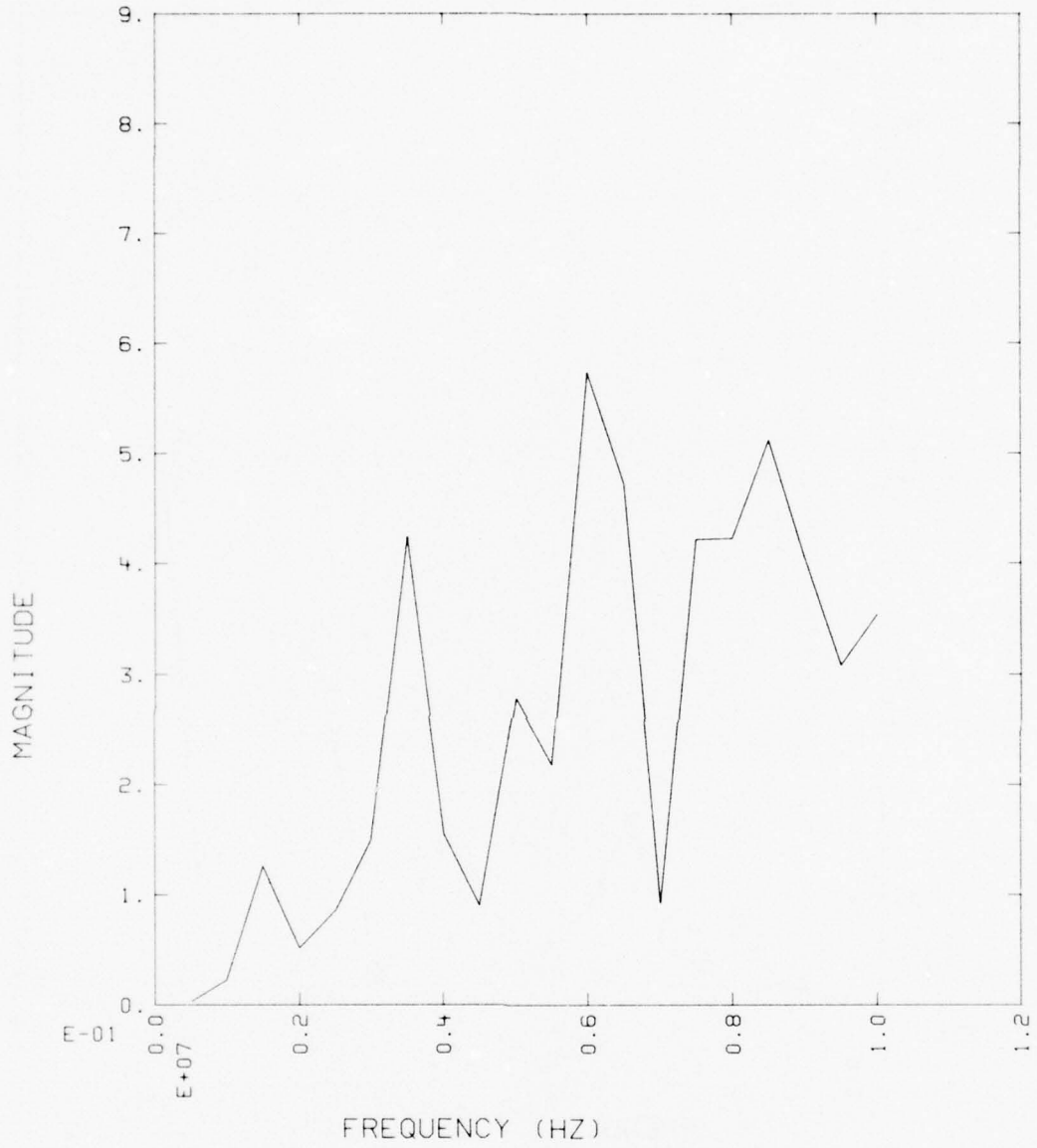

Fig. 4h. The magnitude plot of the calculated identification response for ship-model 3 is shown. This response is found by using the stored library poles for ship-model 3 and the data in Fig. 4b to calculate a set of residues. This set of residues and the stored pole set are then used to calculate a response function at the identification points.

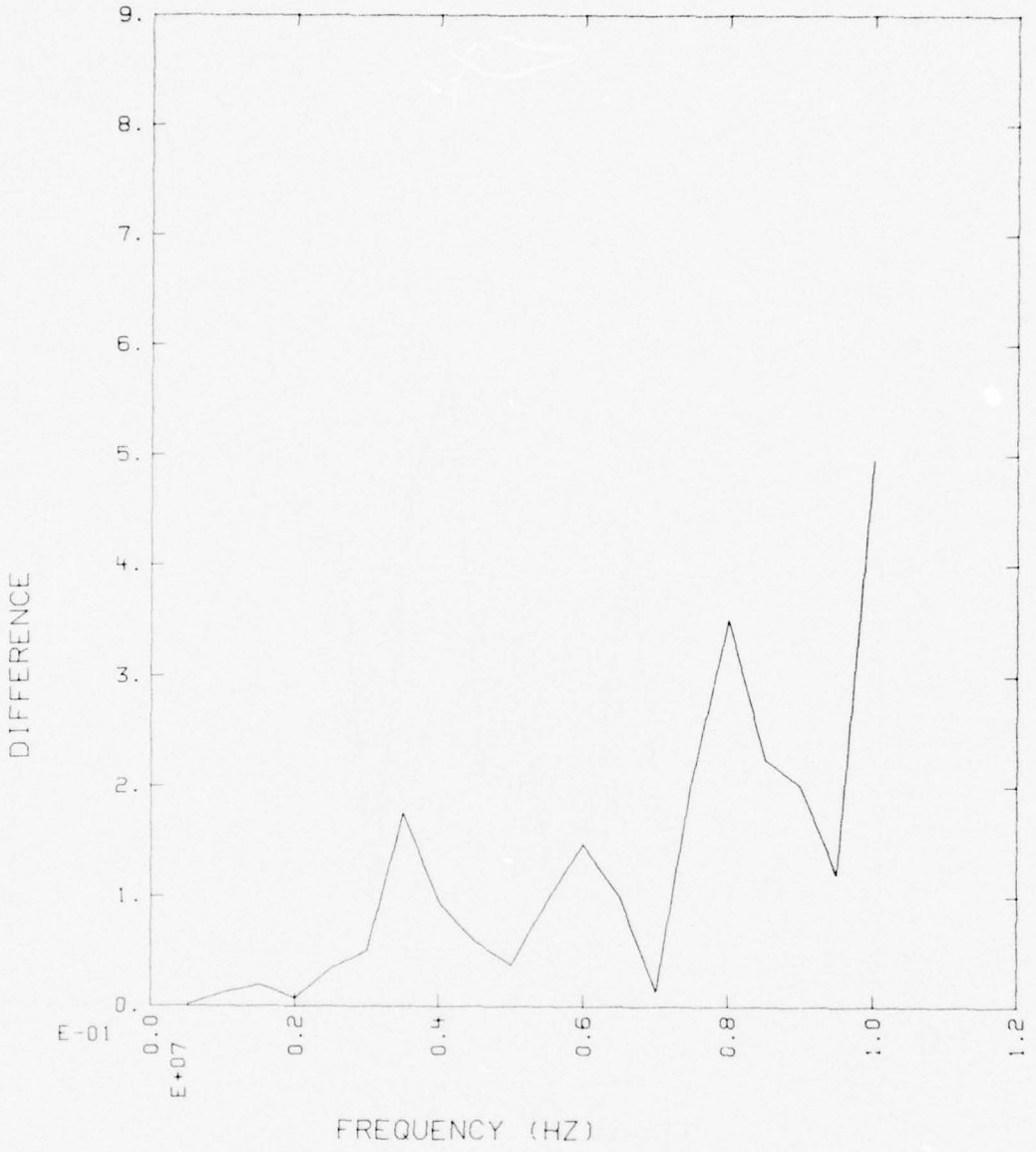

Fig. 4i. The magnitude plot of the difference between the measured and calculated responses at the identification points is shown. This function is found by subtracting the response used to find Fig. 4h from the response used to find Fig. 4c. The identification number [Eq. (4a)] with ship-model 3 is equal to 0.122.

Appendix A

Repeated Processing Cluster Plots

The presence of curve fitting and/or noise poles due to overdetermining the system is difficult to detect in a single calculation from a given data sample. If additional sample sequences are generated from the same waveform (time-domain Prony) or spectrum (frequency-domain Prony), it appears feasible to differentiate between real poles associated with the object and anamolous poles generated by the process.

The additional sequences might arise in several ways. Perhaps the simplest in the frequence domain is the addition to random numerical noise to the original date to generate a new sequence. The invalid poles presumably would move in response to the noise more than would the real poles, thus providing a means for separating them. Repetition of this process several times should produce clusters of real poles and expedite locating them. This technique could tend to degrade the overall process however, and would have to be exercised with care.

An alternate procedure more analogous to what has worked in the time domain would be to develop the additional samples by moving the frequency interval over which the poles are calculated. Again, by repeating this process some number of times, we can identify the valid poles falling in the frequency range overlapped by all intervals.

A third approach possible in the frequency domain would be changing the angle of incidence and/or viewing angle. An advantage of the former is that poles not appreciably excited at the first angle of incidence chosen would be less likely to be missed. The clustered poles that result should be representative of a truly aspect-insensitive pole set, and thus minimize the correlator uncertainty discussed relative to Table 1.

Examples of some of these possibilities are shown in Figs. A-1 to A-3. In Fig. A-1, we present the cluster plots that occur from a fixed bandwidth window being systematically shifted through the spectrum being processed. The target in this case was ship-model 3 for $\theta = 60°$, with data available at 0.125 MHz intervals from 0-10 MHz. A bandwidth of 5 MHz was employed for the pole calculation, resulting in 40 complex data points and 20 pole pairs.

The poles were derived from ten separate calculations by using the frequency intervals $0.125(i + 1)$ to $5 + 0.125i$ MHz, $i = 0,\ldots,9$. Figure A-1 shows the pole sets obtained, where the pole locations are designated by A,..., J corresponding to $i = 0$, $i = 1,\ldots$. Most of the poles actually present in the spectrum are well defined by clusters whose size is that of the individual letters. There is greater variance in some locations, such as for $\omega \gtrsim 5$. Evidently, they are initially outside the window of data. Curve-fitting poles usually seem to scatter rather randomly about the s-plane.

An example of varying the incidence angle, again for ship-model 3, is shown in Fig. A-2. A bandwidth of 0-5 MHz was employed, with 40 frequency samples at 0.125 MHz intervals and 20 pole pairs being extracted. Incidence angles of $\theta = 25°$ to $65°$ in $5°$ steps were employed, and the corresponding pole locations designated by letters A,...,J. For those poles whose location are given by letter-size clusters, the agreement with Fig. A-1 is essentially exact. Curve-fitting poles are made rather obvious by the randomness of their locations.

As the last example of cluster plotting given here, we present in Fig. A-3, the results of using a shifted-frequency window for data contaminated by noise (ship-model 3 at $\theta = 60°$). Cluster plots are shown for three cases of additive, white noise having a maximum value normalized to the peak of the spectal response of ~1.25%, 3.75% and 11.25%, respectively. With increasing noise levels, the locations of valid poles become more uncertain, but the effect depends strongly upon the residue magnitude associated with a given pole. Naturally enough, those poles with the largest residues are least sensitive to a given amount of noise, while poles having residue values near the noise level may disappear. In other words, when the noise is comparable to the magnitude at which a given resonance is excited, that resonance becomes unrecoverable from the data. The rate at which information is lost from a spectrum or waveform as noise increases would be useful to establish in a more quantitative sense. For the shifted-window approach to be successful, uncorrelated noise or a valid noise model is required. This is also true of other methods for processing noisy data. The repetitive processing of such data effectively increases the amount of information available, and thus improves the numerical results that can be obtained.

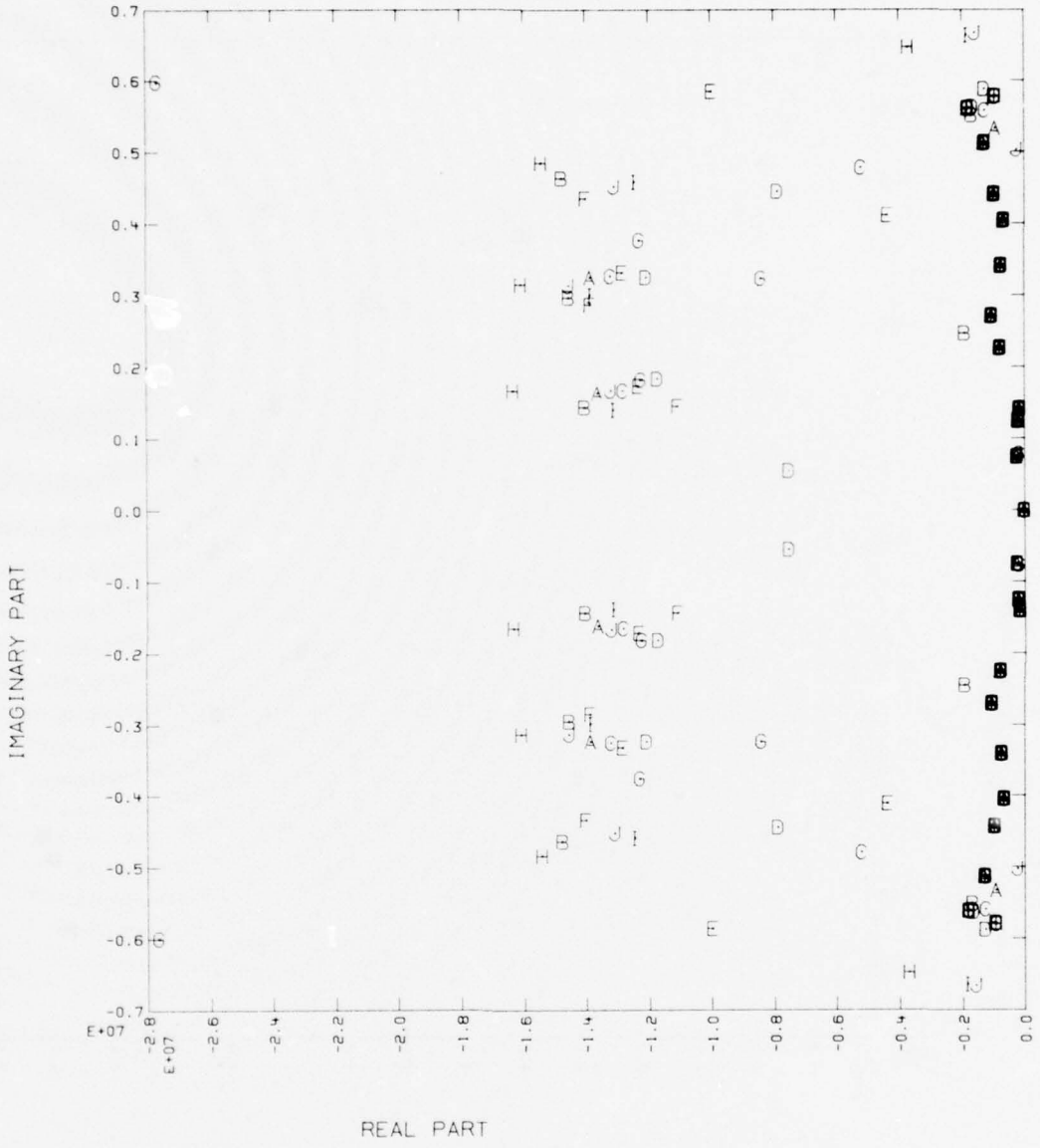

Fig. A-1a. A frequency cluster plot for ship-model 3 at $\theta = 60°$. This plot is produced by using a 5-MHz frequency window, 10 different times on the spectrum data for 0-10 MHz. The poles of each consecutive run are labeled A to J.

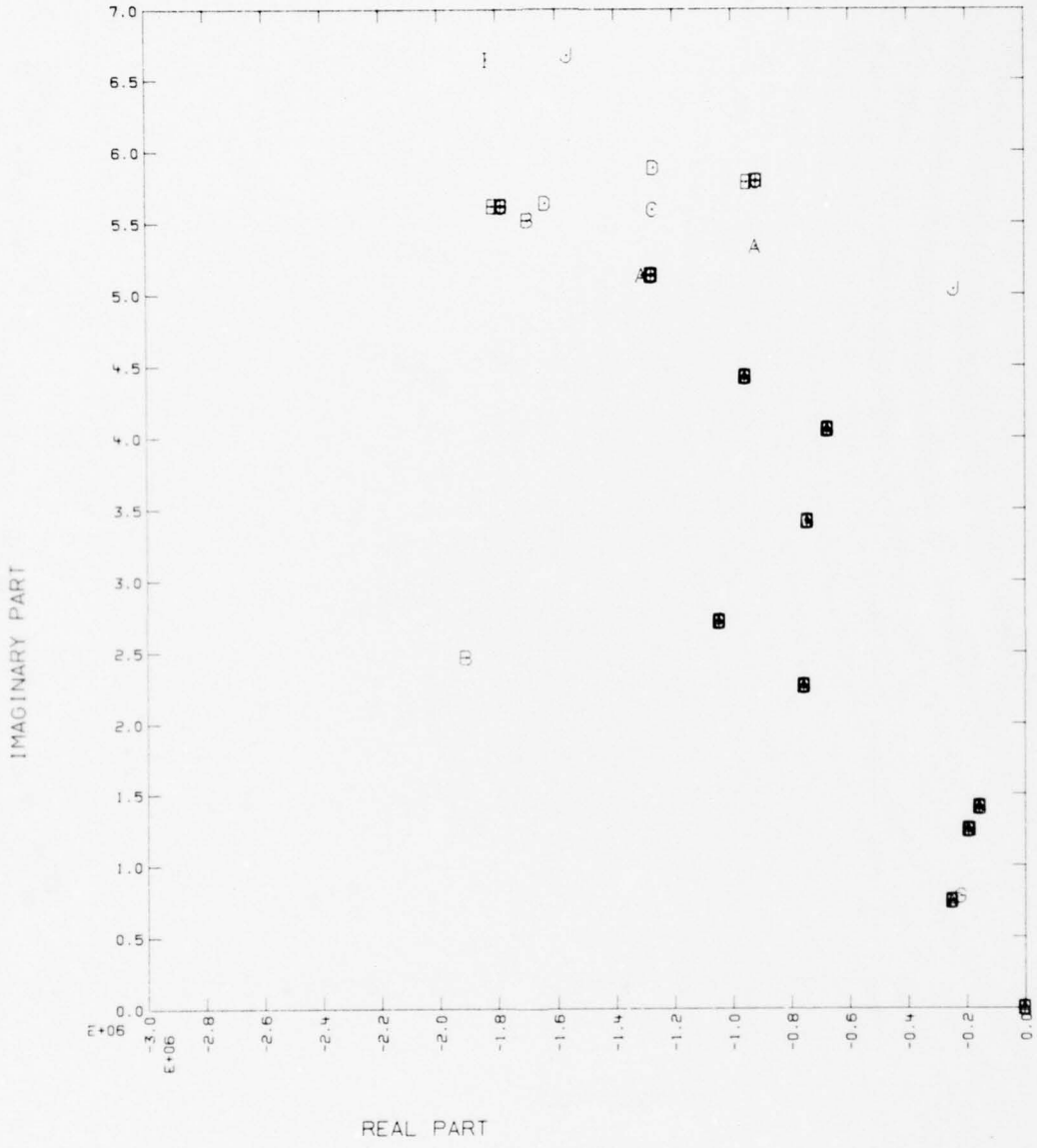

Fig. A-1b. Same as Fig. A-1a, except this figure shows only the second quadrant on an enlarged scale.

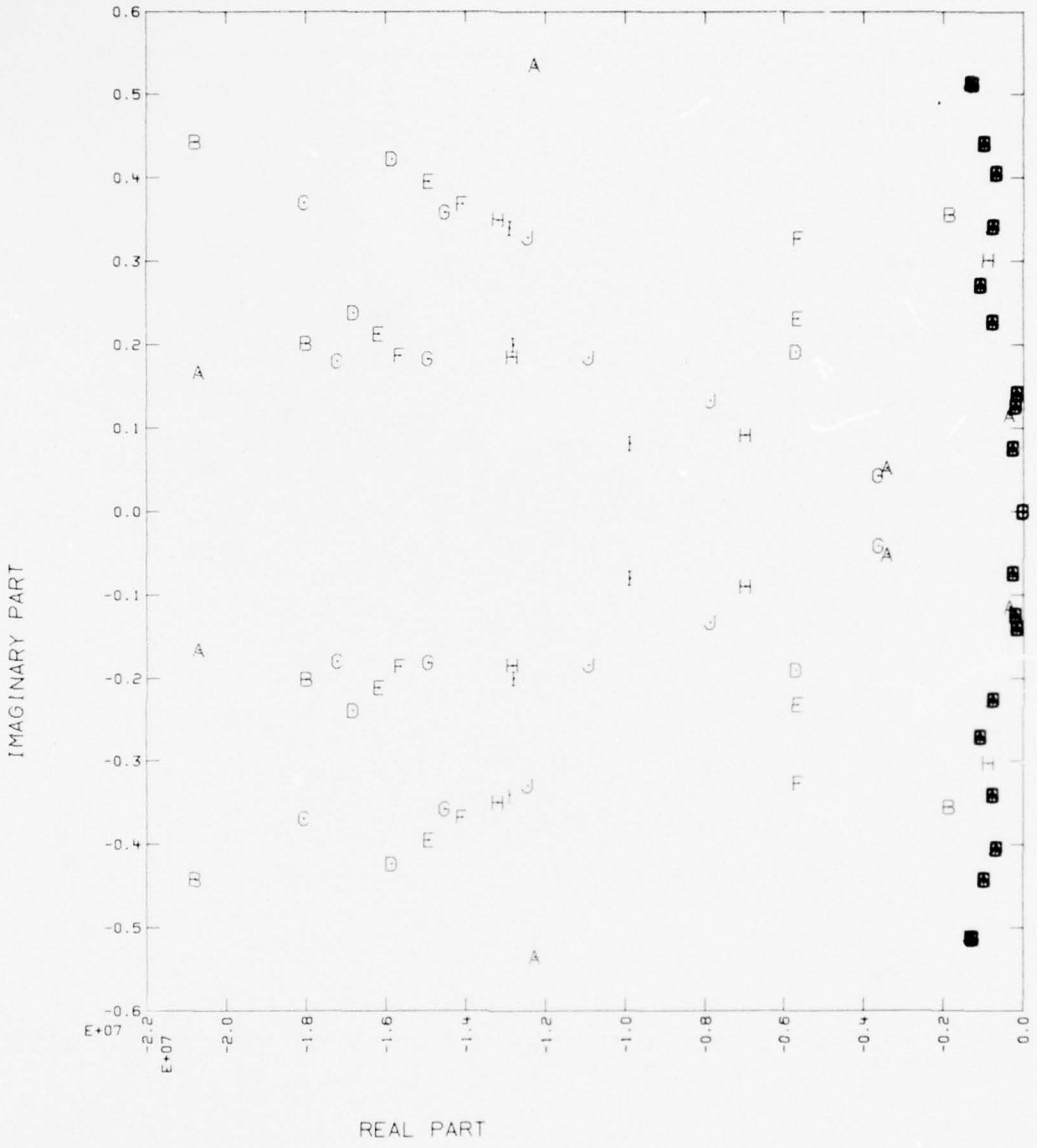

Fig. A-2a. An angular cluster plot for ship-model 3. This plot is produced using the frequency range of 0-5 MHz to obtain the 20 pole pairs but for incidence angles from 25° to 65°. Ten different runs were thus performed and they are lettered from A to J on the plot.

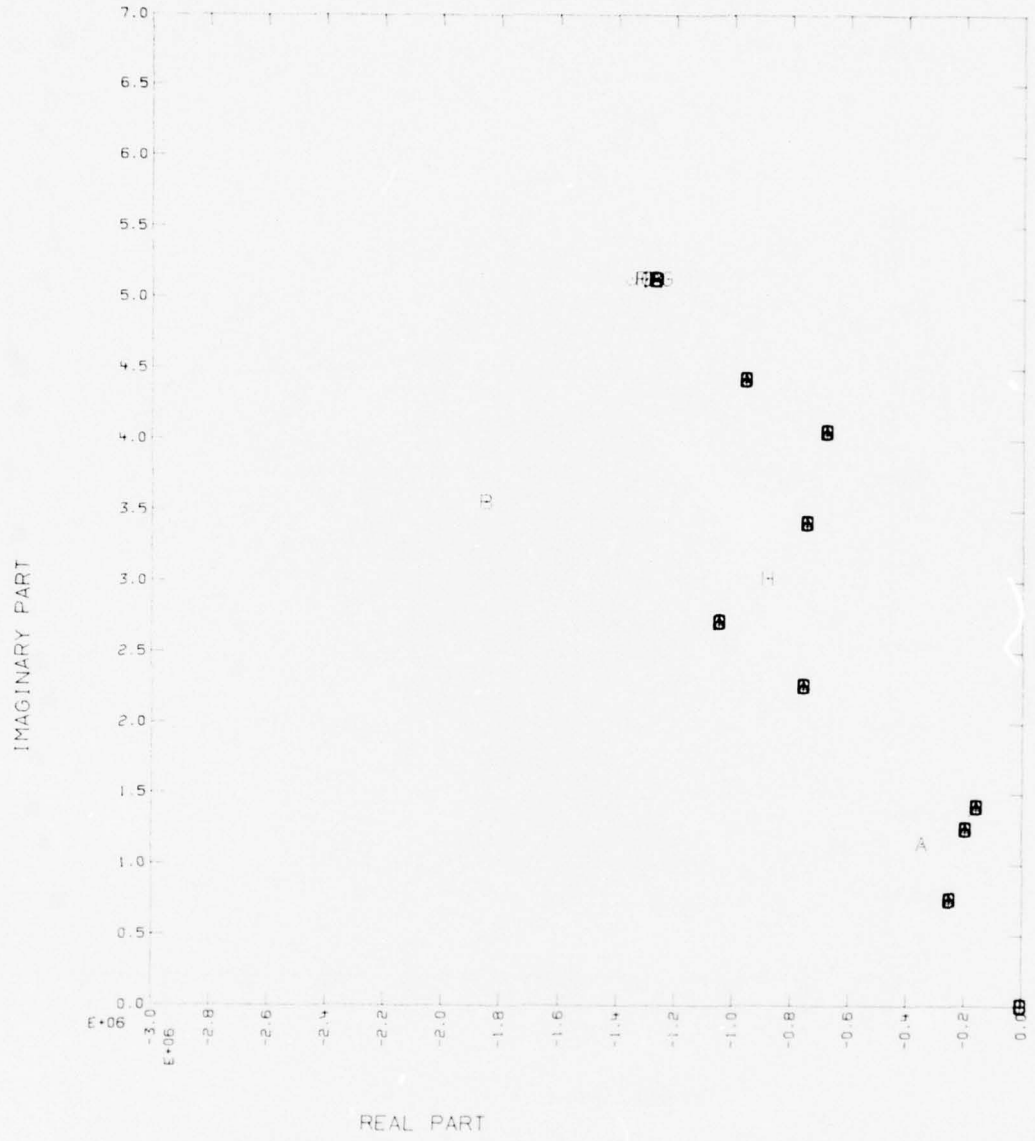

Fig. A-2b. Same as Fig. A-2a, except this figure shows only the second quadrant on an enlarged scale.

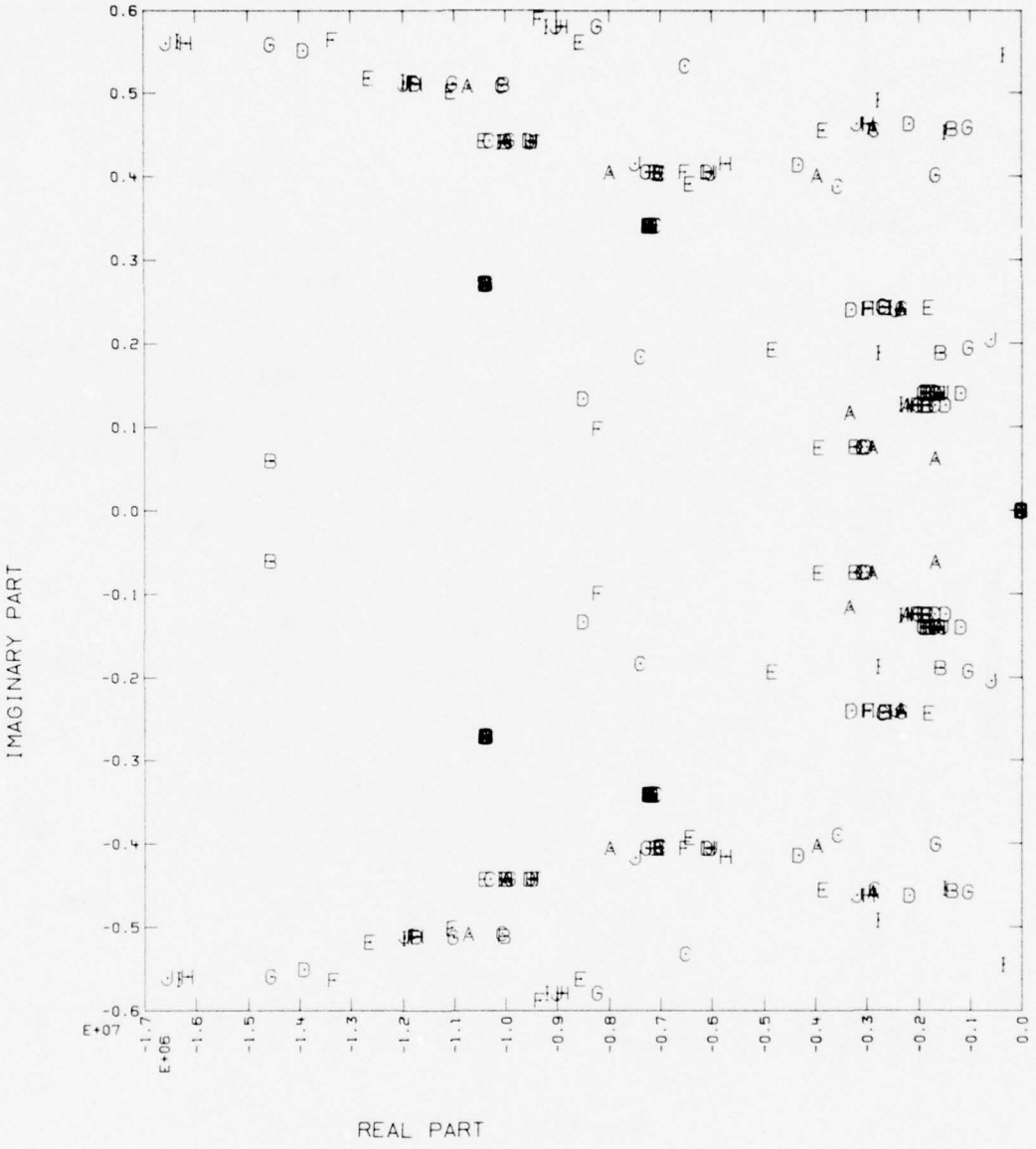

Fig. A-3a. A frequency cluster plot for ship-model 3 at 60° when the data are contaminated by white noise having a maximum value normalized to 1.25% of the spectrum's peak.

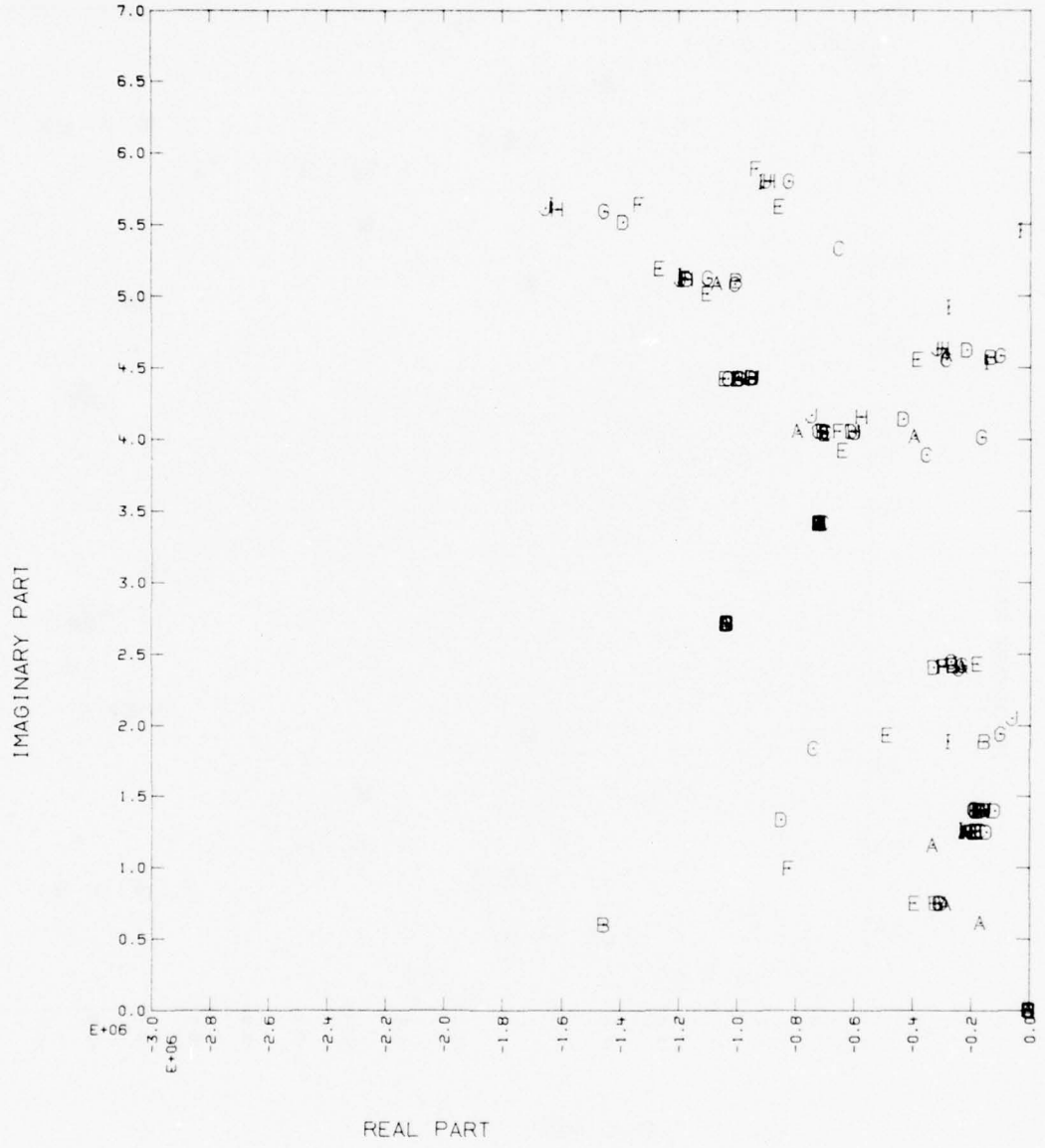

Fig. A-3b. Same as Fig. A-3a, except this figure shows only the second quadrant.

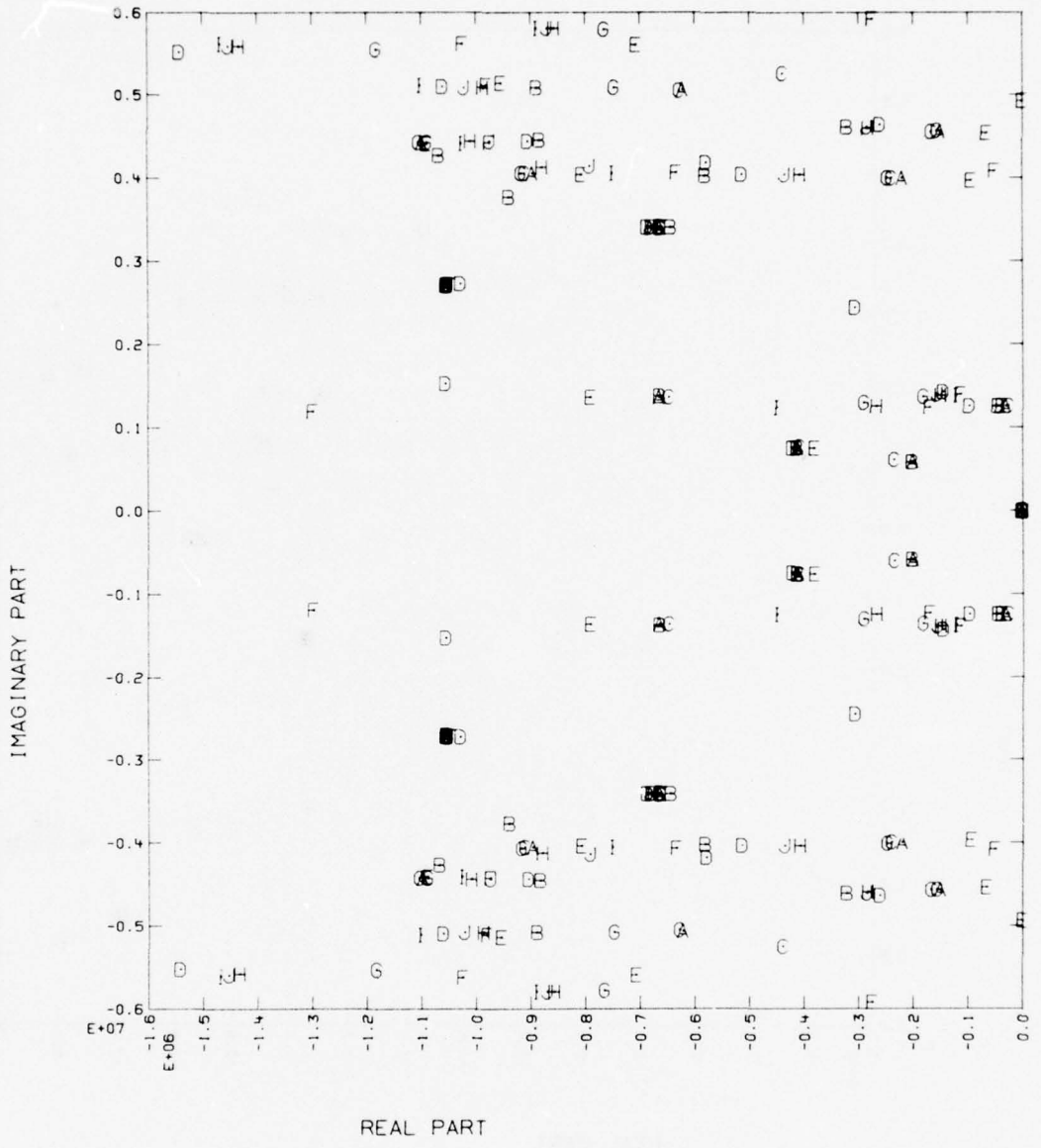

Fig. A-3c. A frequency-cluster plot for ship-model 3 at 60° when the data are contaminated by white noise having a maximum value normalized to 3.75% of the spectrum's peak.

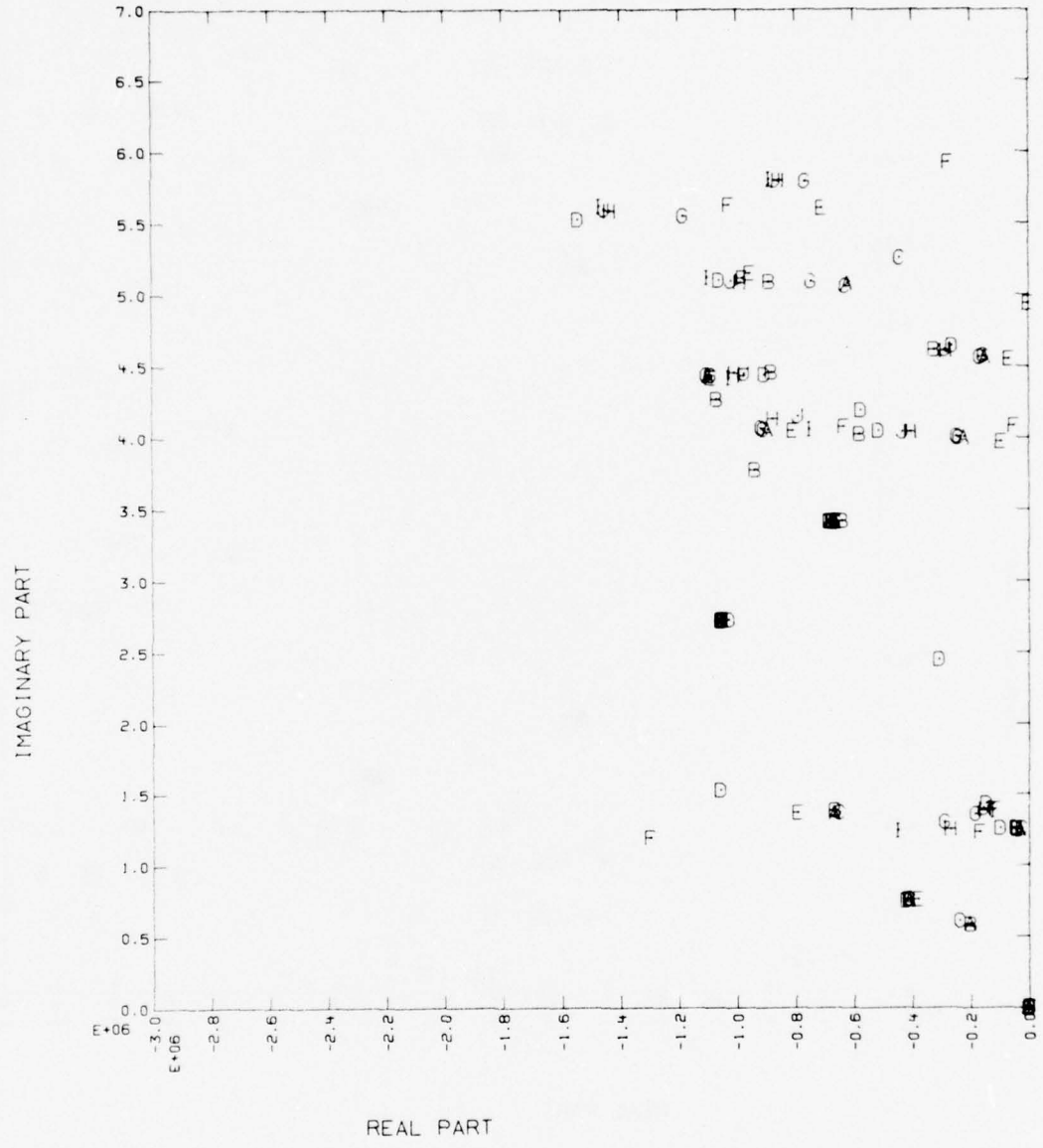

Fig. A-3d. Same as Fig. A-3c, except this figure shows only the second quadrant.

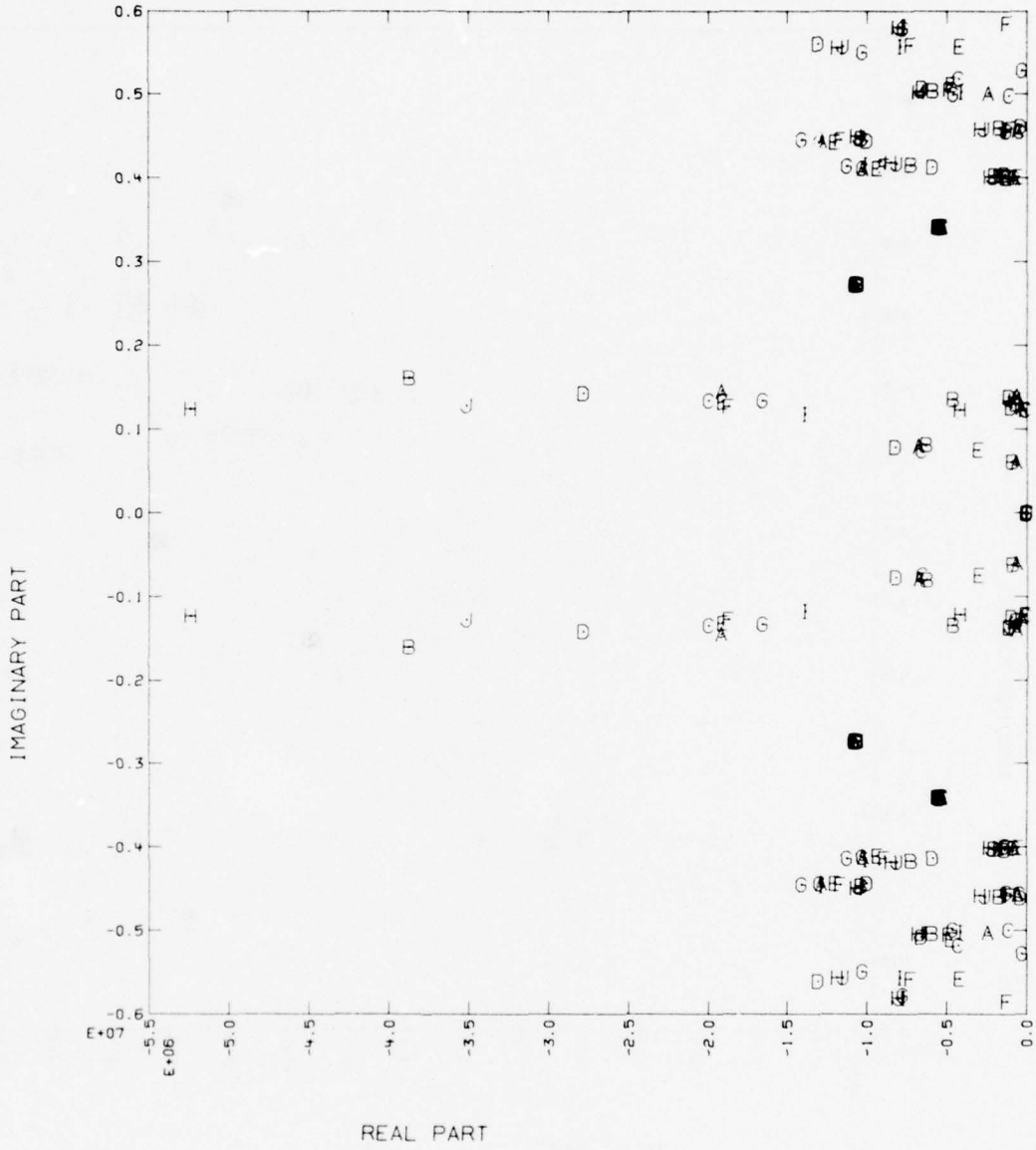

Fig. A-3e. A frequency cluster plot for ship-model 3 at 60° when the data are contaminated by white noise having a maximum value normalized to 11.25% of the spectrum's peak.

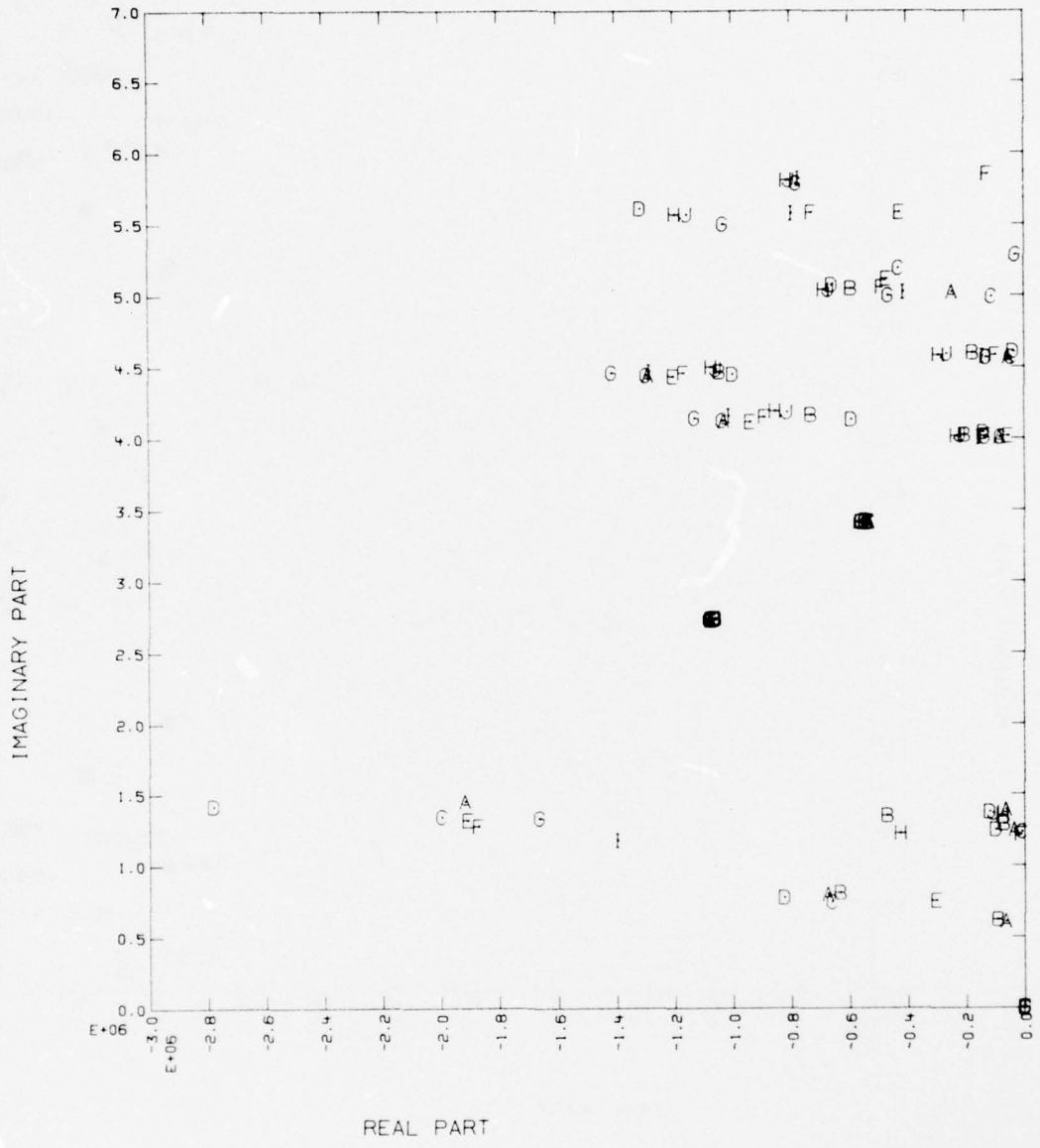

Fig. A-3f. Same as Fig. A-3e, except this figure shows only the second quadrant.

Appendix B
Frequency-Domain Predictors

(E. K. Miller and R. M. Bevensee)

A time-domain linear predictor, as expressed by Eq. (3), requires as data N-constant coefficients $a_{N,\alpha}$, which are determined by the system poles and N-past samples of the time-varying waveform. Once the necessary information is available to put the predictor into operation, all future values of f(t) can be found from repeated application of the predictor. As used in Ref. 6 for object C/I however, only measured data are inserted into the predictor while the computed value at the next time step is used only for correlation. In this way the data used for the prediction are continuously updated, and computation of future values of f(t) involves extrapolation over only one time step. This tends to give equal weight to all the measured data.

A frequency-domain predictor's concept and utility are not so obvious. It is possible to obtain (at least implicity), a frequency-domain predictor that operates in the same way as Eq. (3). The important difference, however, is that its coefficients depend upon frequency; thus, it may be termed a vary-linear predictor (to borrow from system's nomenclature). Its development is indicated below.

First note that the time-and frequency-domain explicit pole representations are

$$f(t) = \sum_{\alpha=1}^{N} R_\alpha e^{s_\alpha t} \underset{\mathcal{L}^{-1}}{\overset{\mathcal{L}}{\rightleftharpoons}} F(j\omega) = \sum_{\alpha=1}^{N} R_\alpha/(j\omega - s_\alpha) \tag{B1}$$

In a similar fashion, their corresponding predictor or implicit representations take the form

$$F(t) = \sum_{\alpha=1}^{N} a_{N,\alpha}(s\beta) f(t - \alpha\Delta t) \rightleftharpoons F(j\omega) = \sum_{\alpha=1}^{N} A_{N,\alpha}(\omega) F(j\omega_\alpha), \tag{B2}$$

where the right hand side of Eq. (B2) has yet to be derived.

There may be several ways to accomplish this. We choose to employ the right-hand side of Eq. (B1), and to obtain the R_α from samples of $F(j\omega_k) = M_k$, $k = 1,\ldots,N$. Thus;

$$R_k = \sum_{\alpha=1}^{N} Y_{k\alpha} M_\alpha , \tag{B3a}$$

where

$$\overline{\overline{Y}} = [\overline{\overline{X}}]^{-1} \text{ and } X_{k\alpha} = (j\omega_k - s_\alpha)^{-1}. \tag{B3b}$$

Formally, this leads to

$$F(j\omega) = \sum_{k=1}^{N} \left(\sum_{\alpha=1}^{N} Y_{k\alpha} M_\alpha \right) / (j\omega - s_k), \tag{B4}$$

which becomes, upon interchanging the order of summation,

$$F(j\omega) = \sum_{\alpha=1}^{N} \left[\sum_{k=1}^{N} Y_{k\alpha} / (j\omega - s_k) \right] M_\alpha . \tag{B5}$$

Thus, from Eqs. (B2) and (B5),

$$A_{N,\alpha}(\omega) = \sum_{k=1}^{N} Y_{k\alpha} / (j\omega - s_k) \tag{B6}$$

Clearly, $A_{N,\alpha}$ is frequency dependent, due to the $j\omega$ term in its denominator. In addition, we observe that since $\overline{\overline{X}}$ depends upon the sequence ω_k, $k = 1,\ldots,N$; any change in the data vector M_k (which thus changes the ω_k) would result in a new matrix $\overline{\overline{X}}$ and thus a new inverse $\overline{\overline{Y}}$. From a computational viewpoint, the latter could be the most costly effect of updating the data since it varies as N^3; whereas, a change in ω results in a N- or N^2-updating process, depending upon whether an explicit [Eqs. (B1) or (B4)] or implicit [Eqs. (B2) or (B5)] form is used. It thus appears that an M-point computation using Eq. (B2) could involve from MN to MN^3 operations, depending upon whether M_k is updated for each computation or not.

However, if the updating is done in a systematic, stepwise fashion, the order of the computation can be decreased. For example, suppose the initial data vector is $M_k^{(1)}$ $(k = 1,\ldots,N)$, the second is $M_k^{(2)}$ $(k = 2,\ldots,N + 1)$, ..., $M_k^{(j)}$ $(k = j,\ldots,N + j - 1)$, where the superscript denotes the step number.

Then, the matrix equivalent of Eq. (B1) at step j is

$$\sum_{\alpha} X_{k\alpha}^{(j)} \; R_{\alpha}^{(j)} = M_{k}^{(j)}, \tag{B7}$$

where $X_{k\alpha}^{(j)}$ depends implicitly upon j through ω_k. But when $j \to j+1$, we note that X is simply changed by deleting the top row ($k = j_{old}$) and adding a new bottom row ($k = j_{new} + N - 1$).

Suppose then the original matrix is conceptually depicted as

$$\overline{\overline{X}}^{(1)} = \begin{bmatrix} X_{11}^{(1)} & X_{12}^{(1)} & \cdots & X_{1N}^{(1)} \\ X_{21}^{(1)} & X_{22}^{(1)} & \cdots & X_{2N}^{(1)} \\ \vdots & & & \\ X_{N1}^{(1)} & X_{N2}^{(1)} & \cdots & X_{NN}^{(1)} \end{bmatrix} \tag{B8}$$

and is solved by Gaussian elimination to obtain the form

$$\overline{\overline{X}}^{(1)'} = \begin{bmatrix} X_{11}^{(1)'} & & & \bigcirc \\ X_{21}^{(1)'} & X_{22}^{(1)'} & & \\ \vdots & & & \\ X_{N1}^{(1)} & X_{N2}^{(1)} & \cdots & X_{NN}^{(1)} \end{bmatrix} \tag{B9}$$

from which the $\overline{\overline{Y}}^{(1)}$ elements can be found by back substitution. If we now introduce the $k = N + 1$ equation while dropping the $k = 1$ equation, we obtain

$$\overline{\overline{X}}^{(2)} = \begin{bmatrix} X_{21}^{(1)'} & X_{22}^{(1)'} & & \bigcirc \\ X_{31}^{(1)'} & X_{32}^{(1)'} & X_{33}^{(1)'} & \\ & & & \\ X_{N1}^{(1)'} & X_{N2}^{(1)'} & \cdots & X_{NN}^{(1)'} \\ X_{N+1,1}^{(2)} & X_{N+1,2}^{(2)} & \cdots & X_{N+1,N}^{(2)} \end{bmatrix} \tag{B10}$$

Upon completing the diagonalization, we find

$$\underline{\underline{X}}^{(2)'} = \begin{bmatrix} X_{11}^{(2)'} & & & \bigcirc \\ X_{21}^{(2)'} & X_{22}^{(2)'} & & \\ | & & \ddots & \\ | & & & \\ | & & & \\ X_{N+1,1}^{(2)} & X_{N+1,2}^{(2)} & \cdots & X_{N+1,N}^{(2)} \end{bmatrix} \tag{B11}$$

a process which involves $\sim N^2/2$ operations.

By induction, we thus conclude that N solutions of a $2N \times N$ system in terms of sequential $N \times N$ subsets will involve $\sim 4N^3/3$ operations in total rather than $\sim N^4/3$ which would result from not exploiting their common equations.

We can summarize the order of the predictor process as follows:

	Explicit		Implicit	
	Updated	Not updated	Updated	Not updated
Time domain	$4N^3/3$	$N^3/3$	$N^3/3$	$N^3/3$
Freq. domain	$4N^3/3$	$N^3/3$	$4N^3/3$	$N^3/3$

Appendix C
Pole and Residue Extraction from Magnitude Data

A method to extract the poles and residue from only the magnitude data of some system response is presented in this appendix. This method is based on the assumption that the response function is causal and positive-real. The positive-real function has all poles and zeros in the left-half plane. The assumption of a positive-real response is only applicable when the system response are from driving-point impedance and admittances. The numerical procedure will first be derived followed by some results of computation.

The response function for an object having only poles and residues can be written as

$$F(s) = \sum_{\alpha=1}^{N} \frac{R_\alpha}{(s - s_\alpha)} , \tag{C1}$$

For the case of casual response, the residues, R_α, and poles, s_α, occur in *complex-conjugate pairs. It has been shown in* Eqs. (3), (4) and (5) of a previous report[2] that (C1) can be written as

$$F(s) = \frac{\sum_{\alpha=0}^{N-1} A_\alpha s^\alpha}{\sum_{\alpha=0}^{N} B_\alpha s^\alpha} , \tag{C2}$$

where A_α and B_α are real numbers, and $B_N = 1$. An alternative form of the same function is

$$F(s) = \frac{d_1 \prod_{\alpha=1}^{N-1} (s - z_\alpha)}{\prod_{\alpha=1}^{N} (s - s_\alpha)} , \tag{C3}$$

where z_α are the zeros of the response and

$$d_1 = A_{N-1} .$$

In Eq. (3) of the previous report[2], it has been shown that

$$A_{N-1} = \sum_{\alpha-1}^{N} s_\alpha . \tag{C4}$$

Therefore, for casual systems, the A_{N-1} are negative real numbers.

The magnitude square of the function can be found by multiplying (C3) by its complex conjugate to obtain

$$|F(j\omega)|^2 = \frac{\sum_{\alpha=0}^{N-1} a_\alpha (j\omega)^{2\alpha}}{\sum_{\alpha=0}^{N} b_\alpha (j\omega)^{2\alpha}}, \tag{C5}$$

where $b_N = 1$. The $(j\omega)$ has been substituted for s in the above equation since the frequency response is known only along the $j\omega$ axis. The a_α and b_α are real coefficients since the A_α and B_α were real.

Note that

$$d_1^2 = A_{N-1}^2 = a_{N-1} . \tag{C6}$$

A different representation for the magnitude square can be found by multiplying (C3) by its complex conjugate and substituting $j\omega$ for s. This new equation is

$$|F(j\omega)|^2 = \frac{-d_1^2 \prod_{\alpha=1}^{N-1} [(j\omega - z_\alpha)(j\omega + z_\alpha^*)]}{\prod_{\alpha=1}^{N} [(j\omega - s_\alpha)(j\omega + s_\alpha^*)]} . \tag{C7}$$

It can be shown from the derivation of (C5) and (C7) that

$$\sum_{\alpha=0}^{N-1} a_\alpha (j\omega)^{2\alpha} = -d_1^2 \prod_{\alpha=1}^{N-1} [(j\omega - z_\alpha)\ (j\omega + z_\alpha^*)], \tag{C8}$$

and

$$\sum_{\alpha=0}^{N} b_\alpha (j\omega)^{2\alpha} = \prod_{\alpha=1}^{N} [(j\omega - s_\alpha)(j\omega + s_\alpha^*)]. \tag{C9}$$

It is obvious from the two above equations that the roots of the two polynomial equations will yield the poles and zeros of the original function. To obtain these roots requires the knowledge of the coefficients in the polynomials.

The coefficients of (C5) can be found by writing this equation in the form

$$-|F(j\omega)|^2 \sum_{\alpha=1}^{N-1} b_\alpha (j\omega)^{2\alpha} + \sum_{\alpha=1}^{N-1} a_\alpha (j\omega)^{2\alpha} = |F(j\omega)|^2 (j\omega)^{2N}. \tag{C10}$$

By evaluating this equation at 2N points along the $j\omega$ axis the coefficients can be expressed as the following set of a linear equations.

$$[A]\ [C] = [G], \tag{C11}$$

where

$$A_{qp} = \begin{cases} -|F(j\omega_q)|^2 (j\omega_q)^{2(p-1)}, & \text{for } q = 1,2,\ldots,2N, \\ & \quad p = 1,2,\ldots,N \\ (j\omega_q)^{2(p-1)-2N}, & \text{for } q = 1,2\ldots,2N, \\ & \quad p = N+1,\ldots,2N; \end{cases} \tag{C12}$$

$$C_q = \begin{cases} b_q & , \text{ for } q = 1,\ldots,N \\ a_{q-n} & , \text{ for } q = N+1,\ldots,2N; \end{cases} \tag{C13}$$

and

$$G_q = (j\omega_q)^{2N} \left|F(j\omega_q)\right|^2; \; q = 1,2,\ldots,2N. \tag{C14}$$

The $\left|F(j\omega_q)\right|^2$ are the values of the magnitude square at the frequence test point $j\omega_q$ which is assumed to be given. The coefficients are found from inverting this set of linear equation.

Once the coefficients b_α are known, the equation

$$\sum_{\alpha=0}^{N} b_\alpha (j\omega)^\alpha = 0 \tag{C15}$$

can be solved for the unknown roots which gives the poles. For causal responses the poles of the response are in the left-half plane. It is obvious from (C9) that the roots of (C15) will be the original, poles plus a reflection of these poles across the $j\omega$ axis. Therefore, the original poles can be found by choosing only those left-half plane poles from the set of all roots of (C15).

Note that up to this point in the derivation only, the only assumption used is that the function is causal. Therefore, the poles of a causal function can be found from the knowledge of magnitude-only data.

Once the coefficients a_α are known, the equation

$$\sum_{\alpha=0}^{N-1} a_\alpha (j\omega)^\alpha = 0 \tag{C16}$$

can be solved for the unknown roots which gives the zeros. For a positive-real responses, the zeros of the response are in the left-half plane. It is obvious from (C8), the roots of (C16) will contain the original system zeros

plus a reflection of these zeros across the jω axis. The original zeros can be found by choosing only those left-half plane zeros from the set of all roots of (C16).

When the poles and zeros of the function are known, the residues of the function remain to be found. To obtain an expression for the residues, begin by equating Eq. (C1) and (C3) to get

$$\sum_{\alpha=1}^{N} \frac{R_\alpha}{(s - s_\alpha)} = \frac{d_1 \prod_{\alpha=1}^{N-1} (s - z_\alpha)}{\prod_{\alpha=1}^{N} (s - s_\alpha)} . \tag{C17}$$

By multiplying both sides of the above equation by $(s - s_q)$ and letting $s = s_q$, we can express the residues as

$$R_q = \frac{d_1 \prod_{\alpha=1}^{N-1} (s - a_\alpha)}{\prod_{\alpha=1}^{N\,q} (s_q - s_\alpha)} , \tag{C18}$$

where the supscript in the product means the deletion of this term when $\alpha = q$. Note from (C6) that $d_1 = -\sqrt{a_{N-1}}$ and the term a_{N-1} has been found in the inversion of (C11).

Before the numerical results of this method are discussed, a possible limitation due to the algebraic structure of the method should be presented. In a previous report[2] where a method was developed to extract poles and residues from the magnitude and phase of the frequency response function, it was shown that the defining equation used to find the coefficients were in powers of n. The similar equation for the magnitude-only method (presented in (C10)) is in powers of 2n. The previous method[2] was shown to work for only 20-pole pairs due to the large dynamic range of the scaled system of linear equations. Since the defining Eq. (C10) is in power of 2n instead of n, the dynamic range of the magnitude-only method should be twice as large as the dynamic range for the method using the magnitude and phase data. Therefore, the magnitude-only

program developed in this appendix should be expected to extract the poles for response that have up to only 10-pole pairs.

A program based on the above was written and tested. The linear Eq. (C11) is solved for the coefficients following which the poles are found by solving for the roots of (C15), and the zeros are found by solving for the roots of (C16). The residues are then found by using Eq. (C18). Some results obtained from this numerical program will not be discussed.

The program was first tested by using a 2-pole-pair, positive-real function. The results for this 2-pole-pair test are shown in Fig. C-1a. This figure shows the given and extracted spectrum and the isometric plot for the given and extracted pole-sets. Also shown in this figure are the tabulations of the given and extracted poles and residues sets. It is obvious from this figure that the technique does work.

The case when a 10-pole-pair, not-positive-real function was used as input data is shown in Fig. C-1b. From this figure one observes that the correct poles are found, but the correct residues were not extracted. Since the response function was causal, the correct poles are expected to be found. The residues found from this program are the residues that fit the poles and coefficient of (C11) in a positive-real sense. This test shown that the method can be used to extract the correct poles from a causal function that is not positive real.

The program was then used to extract poles and residues from the numerical generated data for the driving-point impedance of a 50-meter wire driven at the center. The procedure failed to extract the correct poles and residues from the given data. It found some correct poles; but it also found many incorrect poles. A preliminary investigation into this extraction procedure seem to indicate that the difficulty lay in the root-finding routine. The present root-finding routine is of the type known as Muller's method. This method searches in the complex plane for a root in a rather random fashion, then deflates the original function by the newly found root. The newly deflated function is then searched for a new root. It is suprising that this method of root extraction does not work, since it has been used with great success in the previous reports.[1,2] In these previous tests, the function used had roots only in the left-half plane, but now the function has roots in both half planes. This abundance of roots seems to be confusing the numerical-search procedure used to find the poles and zeros.

A new numerical root-finding routine was obtained that finds roots by method developed by Jenkins and Traub.[12] This method searches in the complex plane for the root with the smallest modulus, then deflates the original function by the newly found root. The newly deflated function is searched for its root having the smallest modulus. The procedure used to search for the roots in this method is different from all previous methods and may be superior.[13] The Jenkins-Traub root-finding routine was in the process of being substituted for the Muller routine when the project terminated.

This appendix has presented a method for extracting the poles from magnitude of causal responses and the poles and residue from magnitude of a position real function. This method should be valid for extracting up to 10 pole-pairs. The method was tested and shown to work for given data, but failed to work on numerically generated EM data. The latter problem apparently stems from the method by which the roots are extracted from the polynomial.

In the future the new Jenkins-Traub root-finding routine should be substituted for the routine using Muller's method to find the roots.

LRS/af/jn/vt/jf

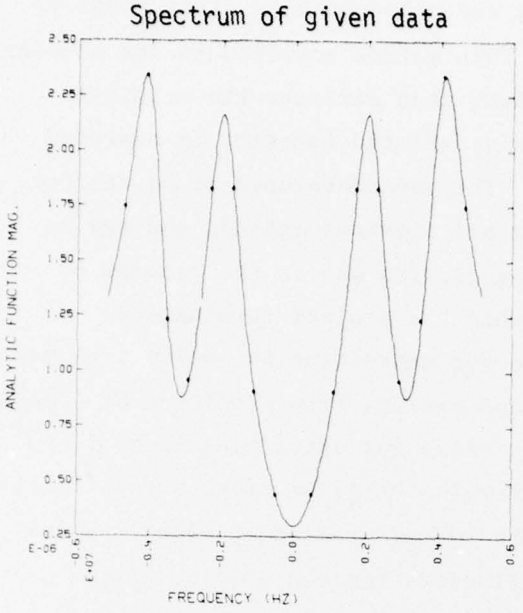

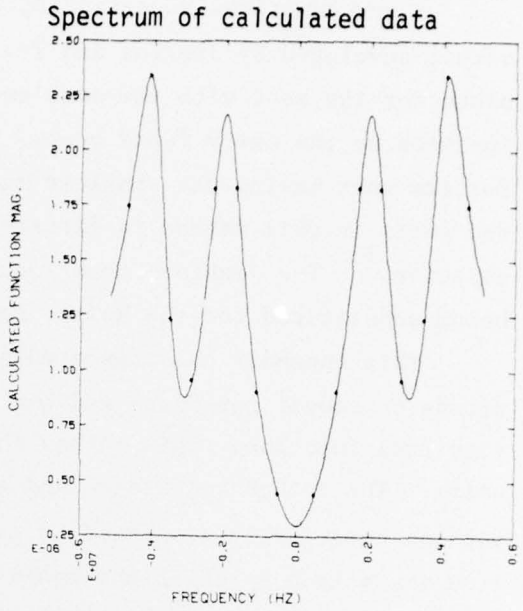

Isometric plot of given poles

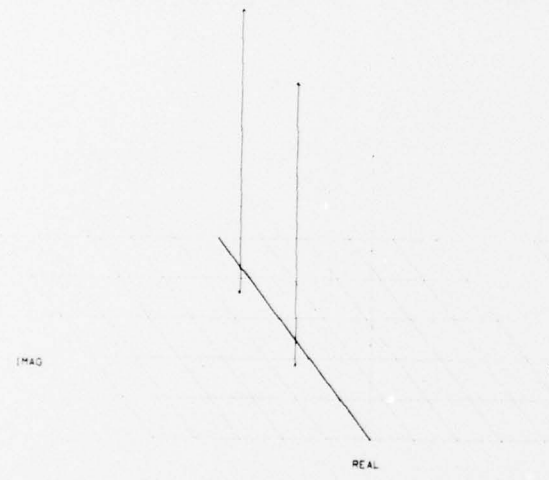

Isometric plot of calculated poles

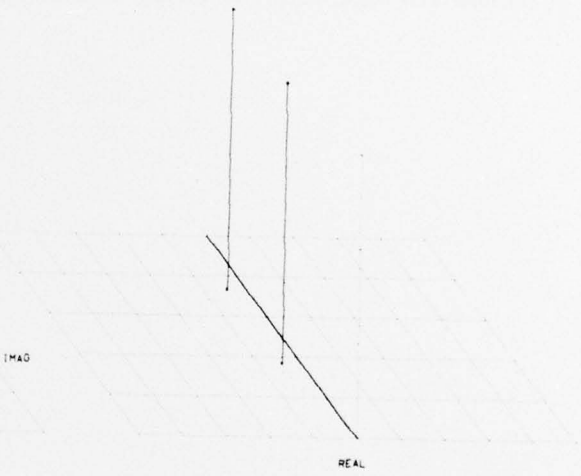

Pole data

	ANALYTIC		CALCULATED	
	REAL PART	IMAG PART	REAL PART	IMAG PART
1	-5.000000E+05	2.000000E+06	-5.000000E+05	2.000000E+06
2	-5.000000E+05	-2.000000E+06	-5.000000E+05	-2.000000E+06
3	-5.000000E+05	4.000000E+06	-5.000000E+05	4.000000E+06
4	-5.000000E+05	-4.000000E+06	-5.000000E+05	-4.000000E+06

Residue data

	ANALYTIC		CALCULATED	
	REAL PART	IMAG PART	REAL PART	IMAG PART
1	1.000000E+00	0.	1.000000E+00	-2.331571E-07
2	1.000000E+00	-0.	9.999998E-01	2.331615E-07
3	1.000000E+00	0.	1.000000E+00	-1.165671E-07
4	1.000000E+00	-0.	9.999999E-01	1.165627E-07

Fig. C-1a. This series shows the results from testing the magnitude-only frequency-domain Prony. This specified transfer function along the jω axis and pole location in the σ-jω plane (with the residue value indicated by the vertical lines) are included. The data shown are for a 2-pole pair, causal, positive-real function.

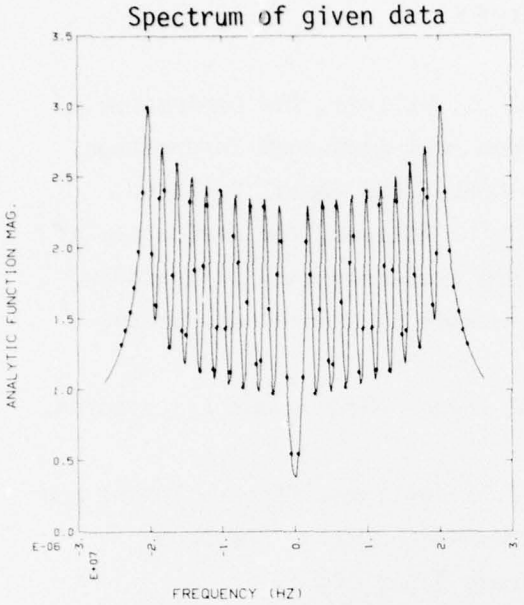

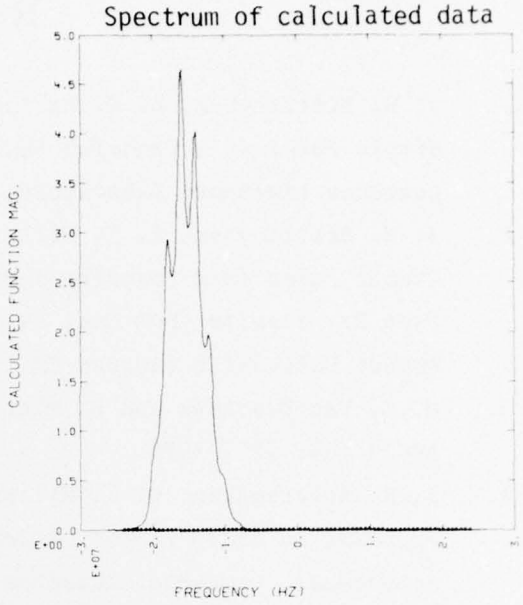

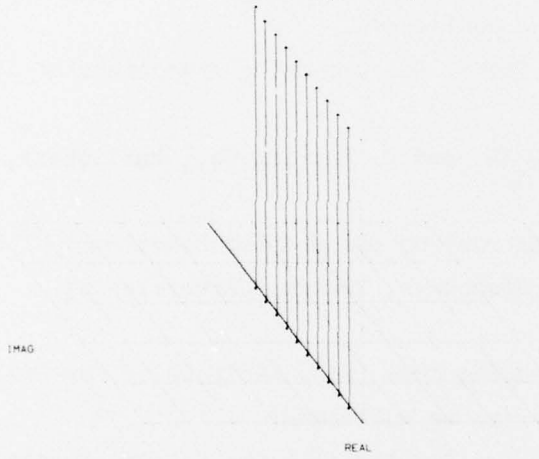

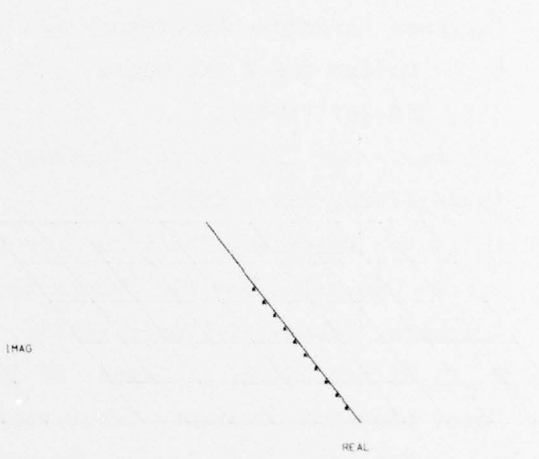

Pole data

	ANALYTIC		CALCULATED	
	REAL PART	IMAG PART	REAL PART	IMAG PART
1	-5.000000E+05	2.000000E+06	-4.998818E+05	2.000146E+06
2	-5.000000E+05	-2.000000E+06	-4.998802E+05	-2.000162E+06
3	-5.000000E+05	4.000000E+06	-5.016571E+05	3.998567E+06
4	-5.000000E+05	-4.000000E+06	-5.007807E+05	-4.003175E+06
5	-5.000000E+05	6.000000E+06	-5.013617E+05	5.997463E+06
6	-5.000000E+05	-6.000000E+06	-5.013577E+05	-5.997427E+06
7	-5.000000E+05	8.000000E+06	-4.964968E+05	7.998859E+06
8	-5.000000E+05	-8.000000E+06	-4.967276E+05	-8.000158E+06
9	-5.000000E+05	1.000000E+07	-5.006825E+05	1.000316E+07
10	-5.000000E+05	-1.000000E+07	-5.006029E+05	-1.000305E+07
11	-5.000000E+05	1.200000E+07	-5.015475E+05	1.199911E+07
12	-5.000000E+05	-1.200000E+07	-5.015788E+05	-1.199908E+07
13	-5.000000E+05	1.400000E+07	-4.994753E+05	1.399955E+07
14	-5.000000E+05	-1.400000E+07	-4.994816E+05	-1.399955E+07
15	-5.000000E+05	1.600000E+07	-4.999019E+05	1.600016E+07
16	-5.000000E+05	-1.600000E+07	-4.999037E+05	-1.600016E+07
17	-5.000000E+05	1.800000E+07	-5.000227E+05	1.800000E+07
18	-5.000000E+05	-1.800000E+07	-5.000248E+05	-1.800000E+07
19	-5.000000E+05	2.000000E+07	-4.999992E+05	2.000000E+07
20	-5.000000E+05	-2.000000E+07	-4.999994E+05	-2.000000E+07

Residue data

	ANALYTIC		CALCULATED	
	REAL PART	IMAG PART	REAL PART	IMAG PART
1	1.000000E+00	0.	-1.100167E-03	1.324966E-03
2	1.000000E+00	-0.	-1.310086E-02	-5.129123E-03
3	1.000000E+00	0.	1.000438E-02	-3.192693E-01
4	1.000000E+00	-0.	7.711696E+00	2.101150E+01
5	1.000000E+00	0.	-5.253521E-01	2.752789E+00
6	1.000000E+00	-0.	-3.240134E+02	-1.736263E+03
7	1.000000E+00	0.	3.362420E+00	-4.104013E+00
8	1.000000E+00	-0.	5.507726E+03	3.372151E+04
9	1.000000E+00	0.	-3.425823E+00	2.167681E-01
10	1.000000E+00	-0.	-5.285476E+04	-2.602288E+05
11	1.000000E+00	0.	3.429261E-01	8.511214E-01
12	1.000000E+00	-0.	2.583651E+05	9.857173E+05
13	1.000000E+00	0.	1.205877E-01	-5.594783E-03
14	1.000000E+00	-0.	-6.618468E+05	-2.030094E+06
15	1.000000E+00	0.	8.735614E-03	-3.546425E-03
16	1.000000E+00	-0.	9.084920E+05	2.316733E+06
17	1.000000E+00	0.	5.253327E-04	3.162872E-04
18	1.000000E+00	-0.	-6.318431E+05	-1.376153E+06
19	1.000000E+00	0.	-1.343589E-04	-1.182113E-05
20	1.000000E+00	-0.	1.745163E+05	3.320201E+05

Fig. C-1b. Same as Fig. C-1a, except the data shown here are for a 10-pole pair, causal, not positive-real function.

References

1. J. N. Brittingham, E. K. Miller, and J. L. Willows, *The Derivation of Simple Poles in a Transfer Function from Real-Frequency Information*, Lawrence Livermore Laboratory, Report UCRL-52050 (April 6, 1976).
2. J. N. Brittingham, E. K. Miller, and J. L. Willows, *The Derivation of Simple Poles in a Transfer Function from Real-Frequency Information, Part 2: Results from Real EM Data*, Lawrence Livermore Laboratory, Report UCRL-52118 (August 23, 1976).
3. M. C. Van Blaricam and R. Mittra, *IEEE Trans. Antenna and Propagation*, AP-23 (6), 777, 1975.
4. J. N. Brittingham, E. K. Miller, and J. L. Willows, *Interim Report and Proposal on Radar Target Characterization via Complex Frequency Resonances*, Lawrence Livermore Laboratory (June 11, 1976).
5. D. Dudley, *Fitting Noisey Data with a Complex Exponential Series*, Lawrence Livermore Laboratory (to be published).
6. D. C. Moffat and R. K. Maine, *IEEE Trans. Antenna and Propagation*, AP-23 (3), 358-367 (1975).
7. *Webster's New Collegiate Dictionary* (G. and C. Merrian Co., Publishers, Springfield, Mass. 1958).
8. M. L. Van Blaricam, *Technique for Extracting the Complex Resonances of a System Directly from its Transient Responses*, Thesis, University of Illinois, Urbana, Illinois (1976).
9. E. K. Miller and D. L. Lager, *EM Imaging from Prony Analysis of Far-Field Data*, Lawrence Livermore Laboratory (to be published).
10. A. A. Ksienshi, "The Inverse Scattering Problem from the Pattern Recognition Point of View," *Proceeding of National Conference on Electromagnetic Scattering* (University of Illinois at Chicago Circle, June 15-18, 1976), pp. 79-82.
11. R. M. Lewis, "Physical Optics Inverse Diffraction," *IEEE Trans. Antenna and Propagation*, AP-17 (3), 308-314 (1969).
12. M. A. Jenkins and J. F. Traub, "A Three-Stage Algorithm for Real Polynomials Using Quadratic Iteration," *SIAM, Numerical Analysis*, vol. 7, No. 4 (December 1970).
13. M. A. Jenkins and J. F. Traub, "Principles for Testing Polynomial Zero-finding Programs," *Meeting on Mathematical Software II* (at Purdue University, May 1974).